

AD-A128 304

TENSION CUTOFF AND PARAMETER IDENTIFICATION FOR THE
VISCOPLASTIC CAP MODEL(U) NOTRE DAME UNIV IN DEPT OF
CIVIL ENGINEERING M G KATONA APR 83 NCEL-CR-83.023

1//

UNCLASSIFIED

N62474-82-C-B270

F/G 8/13

NL

END
DATE
FILED
6-83
DTIC

FORREST V. GAY

Handwritten text in a rectangular box, possibly a list or a set of instructions. The text is illegible due to the high contrast and noise of the scan.

Handwritten text consisting of two lines of repetitive, blocky characters, possibly a barcode or a specific code.

Handwritten text in a rectangular box, similar to the top section, containing illegible characters and possibly a list or instructions.

Unclassified

REPORT DOCUMENTATION PAGE

CR 83.023

TENSION CUTOFF AND PARAMETER IDENTIFICATION FOR THE VISCOPLASTIC CAP MODEL

Final
Dec 1981 - Jan 1982

Dr. Michael G. Kelso

DD-Form 101-1 (Rev. 1-77)

Department of Civil Engineering
University of Notre Dame
Notre Dame, IN 46556

DTIC-001-100

Naval Civil Engineering Laboratory
Port Hueneme, CA 91344

April 1982

Chief of Naval Material
Navy Department
Washington, DC 20380

Unclassified

Approved for public release, distribution unlimited

Elasticity; plasticity; viscoplasticity; CAP75; model; computer program; Crank-Nicolson; geological; explicit; implicit; strain rate; dynamic yield strength; tension cutoff; volumetric stress; deviatoric stress; parameter identification

A viscoplastic formulation based on Perzyna's elastic/viscoplastic theory and the Sandler and Rubin CAP75 plasticity model was extended to include a tension cutoff mechanism. The mechanism employs separate fluidity parameters for the dilatational and deviatoric stress releases. A parameter identification study was performed to determine the sensitivity of the parameters and means of determining them from experimental data.

Unclassified

**TENSION CUTOFF AND PARAMETER IDENTIFICATION
FOR THE VISCOPLASTIC CAP MODEL**

CONTENTS

	<u>Page</u>
PREFACE	1
Background	1
Objective.....	1
Scope	1
PART I. VISCOPLASTIC CAP MODEL WITH TENSION CUTOFF	4
General Review of Viscoplasticity	4
Specialization to Cap Model (Review)	6
Failure Surface	7
Cap Surface	7
Cap Hardening	9
Tension Cutoff Theoretical Development	10
Tension Cutoff.....	11
Exact Solution	12
Numerical Solution Strategy	15
Numerical Approximation	15
Algorithm for Strain Loading	16
Algorithm for Stress Loading	22
Discussion of Tension Cutoff Algorithm	23
Illustrative Example	25
Critique of Tension Cutoff Model	27
Modifications for Viscoplastic Tension Damage....	28
PART II. PARAMETER IDENTIFICATION TECHNIQUES AND EXAMPLES	31
Introduction.....	31
Model Behavior and Influence of Parameters	33
Identification Guidelines	38
Elastic Parameters	38
Failure Surface	38
Cap Surface	39
Cap Hardening	39
Viscous Parameters	40
Tension Cutoff	40



Acquisition For DTIC 1980 2 18 Unannounced Distribution	Distribution/Availability Codes DTIC DTIC and/or DTIC	A
---------------------------------------------------------------------	----------------------------------------------------------------	---

	<u>Page</u>
Parameter Identification using Ideal Experimental Data..	40
Loading Schedules	40
Response Data	41
Identification Procedure	41
Parameter Identification Using Non-Ideal Experimental	
Data	50
Limestone in Triaxial Stress	50
Sedimentary Rock in Triaxial Stress.....	54
Sand in Uniaxial Strain Variable Loading Rate	58
CONCLUSIONS AND RECOMMENDATIONS	65
REFERENCES	68
APPENDIX - VPDRVR PROGRAM: INPUT INSTRUCTIONS	69

PREFACE

Background. This work is a continuation of a previous work effort (1) with the objective of developing a viscoplastic constitutive model for soils and rocks. In the previous work, the inviscid-plastic cap model of Sandler and Rubin (CAP75) was reformulated into a Perzyna-type elastic/viscoplastic model (2). In addition to the theoretical development a numerical solution algorithm was developed to compute six dimensional stress histories from an arbitrary strain loading schedule and vice versa. The algorithm was embodied in the computer program "VPDRVR" which employs a Crank-Nicolson time integration scheme and a Newton-Raphson iterative solution procedure. Numerical studies were performed to validate the program and assess the accuracy for various options of the time integration scheme. The effect of the model fluidity parameters was illustrated for triaxial stress and uniaxial strain loading for a well-studied sand material (McCormick Ranch Sand). Lastly, a finite element solution methodology incorporating the viscoplastic model was presented. It was concluded that the elastic-viscoplastic model shows great promise for capturing the viscoplastic nature of many geological materials. Recommendations for future advancement of the model were to incorporate a viscoplastic tension-cutoff criterion and to establish parameter identification techniques with experimental data. Herein lies the impetus of this study.

Objective. As indicated above, this report addresses two main areas: (1) formulation of a viscoplastic tension-cutoff model to be incorporated into the viscoplastic cap model, and (2) development of parameter identification procedures and guidelines for the cap viscoplastic model.

Scope and Approach. Part I of this report deals with tension cutoff. The underlying motivation for introducing tension cutoff stems from the

recognition that soils and rocks usually exhibit abrupt changes in their stress-strain behavior when loaded in tension, i.e., rapid tensile stress release as micro-cracking or particle separation occurs. To this end, the J_1 (first stress invariant) tension-cutoff criterion proposed by Sandler and Rubin (3) is adopted for this study and recast into viscoplastic formulation. Here, separate fluidity parameters are assigned to the tension cutoff domain to permit independent control on the rate of tensile stress release.

For the sake of completeness, Part I presents a concise review of the viscoplastic cap model prior to introducing the viscoplastic tension cutoff. Following the theoretical tension-cutoff development, a numerical solution algorithm is presented for the entire viscoplastic model including tension cutoff. This algorithm, which predicts stress histories from strain loading and vice versa, is an extension of the previous "VPDRVR" program. Input instructions for the new "VPDRVR" program with tension cutoff is given in the Appendix. Part I concludes with an illustrative example comparing the tension-cutoff numerical solution with an exact solution. Also presented is a critique of the tension-cutoff criterion and recommendations for future enhancements.

Part II of this report addresses the parameter identification problem. We begin by illustrating the influence of various model parameters on the model's performance. With these insights, a set of guidelines are established to aid in parameter identification. For identification purposes, experimental data is classified into two categories "ideal" and "non-ideal". The former implies a well-designed set of experiments especially conceived to ease the identification problem. A hypothetical example of an ideal experiment is presented along with a step-by-step iden-

tification procedure. The "non-ideal" experiments, which sadly enough applies to most existing data, does not lend itself to a "direct" identification procedure. Here a trial-and-error approach using the WPSOL program is suggested and three examples of actual experimental data are investigated.

PART I. VISCOPLASTIC FLOW THEORY AND HARDENING THEORY

Prior to formulating the viscoplastic flow rule and the work hardening theory, review Perzyna's elastic/viscoplastic theory along with the LPTB model developed in the previous work effort (1). This will provide the necessary background for incorporating work hardening.

General Review of Viscoplasticity

Two basic assumptions for the general elastic/viscoplastic theory (2) are, first, the strain-rate vector is composed of elastic and viscoplastic strains, and second, the stress rate vector is related to the elastic strain rate via an elastic (or hyperelastic) constitutive equation. Formally, these assumptions are written as

$$\dot{\epsilon} = \dot{\epsilon}_e + \dot{\epsilon}_{vp} \quad (1)$$

$$\dot{\sigma} = D \dot{\epsilon}_e \quad (2)$$

where $\dot{\epsilon}_e$ and $\dot{\epsilon}_{vp}$ are the elastic and viscoplastic stress rate vectors and D is an elastic constitutive matrix. $\dot{\sigma}$ and $\dot{\epsilon}$ are vector quantities which has a simple time derivative.

A third fundamental assumption is concerned with defining a viscoplastic flow rule relating $\dot{\epsilon}_{vp}$ to the current stress state and a history dependent variable associated with work hardening. This viscoplastic flow rule is expressed as,

$$\dot{\epsilon}_{vp} = \gamma \theta(f) \dot{\epsilon} \quad (3)$$

Here, γ is a material property called the fluidity parameter (units of inverse time) which establishes the relative rate of viscoplastic straining. The scalar function θ (dimensionless) is called the viscous

Flow function and its arguments P is any admissible plastic function
 The function P has to be any admissible plastic function with
 P when $P = 0$, and has the property $P(1) = 1$. This P defines the
 current magnitude of ϵ_{ij} . The current magnitude of ϵ_{ij} is given by the con-
 dition $P = 0$, which is the condition that ϵ_{ij} is of magnitude P which is
 in the reduced normal direction of a 'plastic' yield surface $P = constant = 1$

Similarly, the above definitions refer

$$P(P) = \begin{cases} P(P) & P > 1 \\ 1 & P < 1 \end{cases} \quad \text{plastic flow function} \quad (1)$$

$$P = P(\epsilon_{ij}) \quad \text{plastic flow function} \quad (2)$$

$$n = \frac{\partial P}{\partial \epsilon_{ij}} \quad \text{normal gradient of } P \text{ at } P = 1 \quad (3)$$

The arguments of P and the current stress vector σ_{ij} and ϵ_{ij} are related by
 stress invariants, and a single hardening variable ϵ_{ij} which is defined
 by some integral hardening function of the plastic work done
 history, i.e., $\epsilon_{ij} = \int \epsilon_{ij}$. For a given value of ϵ_{ij} all values of stress
 that satisfy $P(\sigma_{ij}, \epsilon_{ij}) = 1$ form the current 'plastic' yield surface in a
 classical plasticity yield surface. In terms of the stress and strain
 forms a boundary behavior of plastic $P = 1$ and a rigid part $P < 1$ forms
 when a constant stress state is imposed and then $P = 1$ always plastic flow or
 occur and continue to occur at a constant rate of $P = 1$ as a hardening yield
 function. If P is a hardening function, as a plastic flow occurs at a
 decreasing rate because, as a plastic flow occurs, ϵ_{ij} changes
 in value such that $P(\sigma_{ij}, \epsilon_{ij}) = 0$, hence $\epsilon_{ij} = 1$. In other words, the origi-
 nal static yield surface 'moves out' at a rate that leads to eventually
 form a new static yield surface containing the imposed stress state. Once
 this has occurred, we say the solution is steady state (since $\dot{\epsilon}_{ij} = 0$), and

the resulting accumulated strains would be identical to the corresponding inviscid plasticity solution.

With the foregoing assumptions and concepts, a general viscoplastic constitutive relation is readily obtained by combining Equations 1 and 2 to get

$$\dot{\epsilon} = \frac{2}{3} \dot{\epsilon}_0 \left(\frac{\sigma}{\sigma_0} \right)^n \quad (7)$$

Or upon replacing $\dot{\epsilon}_0$ with Equation 3, we have

$$\dot{\epsilon} = \frac{2}{3} \dot{\epsilon}_0 \left(\frac{\sigma}{\sigma_0} \right)^n \quad (8)$$

Note, although $\dot{\epsilon}_0$ is inferred in the hardening argument of the last equation, $\dot{\epsilon}_0$ is still here $\dot{\epsilon}_0 = \dot{\epsilon}$ so that Equation 8 implicitly provides the desired $\dot{\epsilon}$ relationship in a differential form.

Specialization to Creep Model (Review)

To specialize the foregoing viscoplastic constitutive relationships for soils and rocks, functional forms for μ , F , and $\dot{\epsilon}_0$ must be defined along with the components of the elasticity matrix \mathbf{C} . Here, we review the forms established in the previous viscoplastic creep model without tensor cutoff. These forms are valid whenever the stress state satisfies the cap or failure surface. Modification of these forms to include tensor cutoff is presented after this review.

Two optional forms for the viscoplastic flow function are

$$a) F = \left(\frac{\sigma}{\sigma_0} \right)^N \quad (9)$$

$$b) F = \exp \left(\frac{\sigma}{\sigma_0} \right) - 1 \quad (10)$$

where N is an exponent and σ_0 is a normalizing constant with the same units as σ so that F is dimensionless (N may be considered as a material property).

Although more elaborate functional forms for ϕ may be established (2), the forms given by Equations 9 and 10 appear to suffice for many geological materials (4,5).

Specification of the plasticity yield function f is patterned after the inviscid cap model (3) wherein J_1 , the first stress invariant, and J'_2 , the second deviator stress invariant, are used to define the current static yield surface, as illustrated in Figure 1. Here, the static yield surface is divided into three regions along the J_1 axis; the failure surface region ($T > J_1 > L$), the cap surface region ($J_1 \leq L$), and the tension-cutoff region ($J_1 \geq T$).

Failure Surface. The failure surface is a non-hardening, modified Drucker-Prager form with a yield function defined by:

$$f_F(J_1, J'_2) = \sqrt{J'_2} - (A - C \exp(BJ_1)) \quad (11)$$

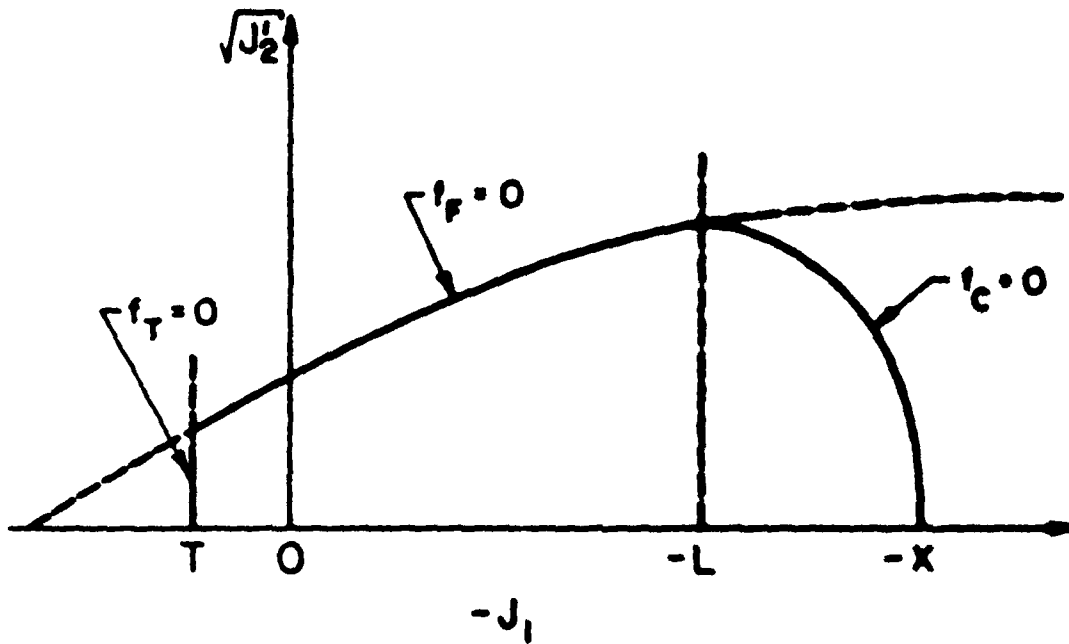
where A , B , and C are plastic material constants ($A > C$). This yield function is used to define viscoplastic flow (Equation 3) whenever J_1 is in the range $T > J_1 > L$. The failure surface forms a boundary along which the cap surface can move (harden/soften).

An alternative form for f_F is the standard Drucker-Prager surface given by:

$$f_F(J_1, J'_2) = \sqrt{J'_2} - (A - BJ_1) \quad (12)$$

where A and B are material constants. The first form is generally preferable.

Cap Surface. The cap surface is a hardening surface in the shape of an ellipse quadrant when plotted in $J_1, \sqrt{J'_2}$ space (Figure 1). It is defined in a "squared" form with the normalizing constant f_0 (stress unit) as:



$$f(\sigma, \bar{\epsilon}) = \begin{cases} f_T(J_1), & J_1 \geq T \text{ (Tension)} \\ f_F(J_1, J_2'), & T > J_1 > -L \text{ (Failure)} \\ f_C(J_1, J_2', \bar{\epsilon}), & J_1 \leq -L \text{ (Cap)} \end{cases}$$

Figure 1. Illustration of steady-state plasticity surfaces for cap model.

$$f_c(J_1, J_2, \dot{\epsilon}) = (J_2 - \lambda) - \sqrt{A^2 - (J_1 - L)^2} - \dot{\epsilon}^D \quad (13)$$

The variable cap parameters L and λ are positions on the J_1 axis which locate the current cap surface ($f_c = 0$) in (J_1, J_2) space. The coordinate point $(L, \sqrt{A^2 - (J_1 - L)^2})$ is where the cap surface intersects the failure surface. L and λ are related by the positive material parameter β which defines the ratio of the principal ellipse radii forming the cap surface, i.e.

$$L - \lambda = \beta \sqrt{A^2} \quad (14)$$

where $\sqrt{A^2} = A = C \exp(\beta L)$ is the vertical ellipse radius and $\beta = b$ is the horizontal ellipse radius. Typically β is specified as a constant. More generally, however, β may be a specified function of L . (e.g., see Appendix A)

Cap Hardening. Hardening of the cap surface is controlled through an auxiliary hardening function $\lambda = \lambda(\dot{\epsilon})$ where $\dot{\epsilon}$ is an accumulation of compressive, volumetric, viscoplastic strain increments. It is given by

$$\lambda(\dot{\epsilon}) = \ln(\dot{\epsilon}/W + 1)/D \quad (15)$$

where W and D are positive material hardening constants. Upon loading the cap ($J_1 < L$), the hardening argument $\dot{\epsilon}$ is an accumulation of negative increments given by

$$\dot{\epsilon} = \dot{\epsilon}_0 + \int_0^t \dot{\epsilon} dt \quad (16)$$

$$\text{where } \dot{\epsilon} = \min(\dot{\epsilon}_{vp11}, \dot{\epsilon}_{vp22}, \dot{\epsilon}_{vp33}, 0) \quad (17)$$

Initially the cap is located by specifying $\lambda = \lambda_0$. Typically with a small negative value near the J_1 origin. This in turn provides the initial values of L (Equation 14) and $\dot{\epsilon}_0$ (Equation 15). Upon loading the cap, i.e., $J_1 < L$ and $f_c > 0$, viscoplastic flow occurs which negatively increases $\dot{\epsilon}$, λ , and L ; thereby expanding the cap as it moves in the $-J_1$

direction.

Additional hardening rules for soils have been developed which permits the cap to retract when loading on the failure surface or tension surface in order to limit excessive dilatancy. This retraction is more akin to kinematic hardening rather than strain softening. Thus for soils (not rocks), $\dot{\epsilon}_c$ may take on positive increments values when $J_1 > 1$ (failure or tension surface loading) according to the relationship:

$$\dot{\epsilon}_c = \max \left\{ \dot{\epsilon}_c, \frac{1}{2} \left(\frac{dJ_1}{dt} - \dot{\epsilon}_c \right) \right\} \quad (18)$$

When this increment is accumulated in Equation 16, $\dot{\epsilon}_c$ becomes less negative, retracting the cap. However, $\dot{\epsilon}_c$ is limited in positive growth such that the cap parameter L does not become greater than the current value of J_1 . Hence the maximum value of $\dot{\epsilon}_c$ when loading the failure or tension surface is

$$\dot{\epsilon}_c = W(\exp(D\lambda_c) - 1) \quad (19)$$

where λ_c is determined from Equation 14 by letting $L = J_1$, i.e. $\lambda_c = J_1 - R_0 \sqrt{J_2}$.

This special hardening rule for soils helps to limit excessive dilatancy (i.e., volumetric expansion inherently associated with loading the failure and tension surfaces) by allowing the cap to be activated sooner when subsequent compression loading is encountered.

Another restriction imposed on $\dot{\epsilon}_c$ is that it is never allowed to become greater than its initial value $\dot{\epsilon}_c^0$.

The foregoing completes the viscoplastic cap model review and sets the stage for formulating the viscoplastic tension-cutoff model.

Tension Cutoff Theoretical Development.

In this section we present a viscoplastic tension-cutoff model

employing the same tension failure criterion proposed by Sandler and Rubin for the inviscid cap model (3). Although their criterion does not conform to any rigorous fracture theory, it is believed to be appropriate for the purpose of rapidly reducing the stiffness of those elements experiencing tension. Further critique and extensions of the tension cutoff model are given in the concluding portion of this development.

Tension Cutoff. The tension-cutoff criterion employed in the inviscid cap model is triggered when $J_1 = T$. Here, T is a material constant representing the threshold of volumetric tension stress at which abrupt stress releases occur due to tension damage. Specifically, whenever a stress state is encountered such that $J_1 > T$, it is assumed that all deviatoric stresses vanish instantaneously, and the volumetric stress in excess of T vanishes. Thus, the final inviscid stress state is $\sigma_{11} = \sigma_{22} = \sigma_{33} = T/3$, all other $\sigma_{ij} = 0$.

Putting this tension cutoff criterion into a viscoplastic form infers the stresses are released at a rate controlled by the fluidity parameter γ rather than an instantaneous release. Accordingly, it is reasonable to specify γ in the tension region (say γ_T) at a higher value than the value of γ in the failure/cap regions. Moreover, since the tension cutoff criterion treats volumetric and deviatoric stress releases independently the viscoplastic strain rate must be independently defined in terms of volumetric and deviatoric strain-rate components.

With the above understanding, the viscoplastic tension cutoff model is defined by the following. The plasticity yield function for tension cutoff, f_T , is given by:

$$f_T(J_1) = J_1 - T \quad (20)$$

Hence, the "static" yield surface ($f_T = 0$) is a stationary vertical line, $J_1 = T$, as shown in Figure 1. When $f_T < 0$, tension cutoff is triggered and the viscoplastic strain rate is defined by:

$$\dot{\epsilon}_{vp} = \gamma_T \psi(f_T) \mathbf{m}_T + \gamma_G \psi(f_G) \mathbf{m}_G \quad (21)$$

where

$$\gamma_G = \frac{1}{\sqrt{3}} \frac{d\gamma_G}{df_G}$$

$$\mathbf{m}_G = \frac{\partial \mathbf{f}_G}{\partial \boldsymbol{\sigma}} = \frac{1}{2\sqrt{J'_2}} \begin{bmatrix} \sigma_{11} & \sigma_{22} & \sigma_{33} & 2\sigma_{12} & 2\sigma_{13} & 2\sigma_{23} \end{bmatrix}^T$$

$$\mathbf{m}_T = \frac{\partial f_T}{\partial \boldsymbol{\sigma}} = \begin{bmatrix} 1 & 1 & 1 & 0 & 0 & 0 \end{bmatrix}^T$$

Equation 21 is a modified form of the viscoplastic flow rule corresponding to Equation 3. Here the first right-hand-side term contains the viscoplastic strain-rate for volumetric components, and the second term contains the deviatoric components. The two tension fluidity parameters, γ_T and γ_G , permit independent control of the volumetric and deviatoric stress release rates, respectively.

As a conceptual illustration, consider a material that is suddenly strained producing an instantaneous elastic stress state such that $f_T(J_1) > 0$. This induces viscoplastic flow (Equation 21) which in turn releases stresses until $\dot{\epsilon}_{vp} = 0$. When this occurs, we have the steady state condition; $f_T = f_G = 0$, or $J_1 = T$ and $J'_2 = 0$, thereby satisfying the tension-cutoff criterion.

Exact Solution. A deeper understanding of the tension-cutoff model can be achieved by obtaining an exact solution and studying its behavior. An exact solution can be obtained for a specified strain loading by decomposing the stress vector and elastic matrix into volumetric and deviatoric components and solving the uncoupled system. To this end, the stress vector is written as:

$$\underline{\sigma} = \underline{\nu} + \underline{s} \quad (22)$$

where, $\underline{\nu} = \frac{1}{3} J_1 < 1, 1, 1, 0, 0, 0 >^T$ = volumetric stress components

and $\underline{s} = < s_{11}, s_{22}, s_{33}, \sigma_{12}, \sigma_{13}, \sigma_{23} >^T$ = deviatoric stress components

Accordingly, the elastic matrix is decomposed into bulk and shear components as:

$$\underline{D} = \underline{K} + \underline{G} \quad (23)$$

where, $\underline{K} = K_0$

$$\begin{bmatrix} 1 & 1 & 1 & 0 & 0 & 0 \\ & 1 & 1 & 0 & 0 & 0 \\ & & 1 & 0 & 0 & 0 \\ \text{sym} & & & 0 & 0 & 0 \\ & & & & 0 & 0 \\ & & & & & 0 \end{bmatrix} = \text{bulk modulus components}$$

and, $\underline{G} = \frac{G_0}{3}$

$$\begin{bmatrix} 4 & -2 & -2 & 0 & 0 & 0 \\ & 4 & -2 & 0 & 0 & 0 \\ & & 4 & 0 & 0 & 0 \\ \text{sym} & & & 3 & 0 & 0 \\ & & & & 3 & 0 \\ & & & & & 3 \end{bmatrix} = \text{shear modulus components}$$

Now the basic constitutive relationship, i.e., the equivalent of Equation 7, can be expressed in two sets of equations:

$$\dot{\underline{\nu}} = \underline{K}(\dot{\underline{\epsilon}} - \dot{\underline{\epsilon}}_{vp}) \quad (24)$$

$$\dot{\underline{s}} = \underline{G}(\dot{\underline{\epsilon}} - \dot{\underline{\epsilon}}_{vp}) \quad (25)$$

Upon replacing $\dot{\underline{\epsilon}}_{vp}$ in the above with tension flow rule (Equation 21) we have:

$$\dot{\underline{\nu}} = \underline{K} \dot{\underline{\epsilon}} - \gamma_T \phi(f_T) \underline{K} \underline{m}_T \quad (26)$$

$$\dot{\underline{s}} = \underline{G} \dot{\underline{\epsilon}} - \gamma_G \phi(f_G) \underline{G} \underline{m}_G \quad (27)$$

Note, the uncoupling in the last two equations is due to the fact that $\underline{K} \underline{m}_G = \underline{G} \underline{m}_T = 0$.

If the viscous flow function ϕ is taken in its simplest linear form, i.e. $\phi(f_T) = (J_1 - T)/f_0$, and $\phi(f_G) = \sqrt{J_1^2}/f_0$, then Equations 26 and 27 become the following first order, linear differential, vector equations:

$$\dot{\underline{v}} + \left(\frac{9K_0 \gamma_T}{f_0} \right) \underline{v} = \underline{K} \dot{\underline{\epsilon}} + \left(\frac{3TK_0 \gamma_T}{f_0} \right) \underline{m}_T \quad (28)$$

$$\dot{\underline{s}} + \left(\frac{G_0 \gamma_G}{f_0} \right) \underline{s} = \underline{G} \dot{\underline{\epsilon}} \quad (29)$$

In arriving at the above, use is made of the relations, $\underline{v} = \frac{J_1}{9K_0} \underline{K} \underline{m}_T$ and $\underline{s} = \frac{\sqrt{J_1^2}}{G_0} \underline{G} \underline{m}_G$.

A solution may be obtained for the case of a stepped strain loading, $\underline{\epsilon}(t) = \underline{\epsilon}^* h(t)$, where $\underline{\epsilon}^*$ is any constant strain vector causing initial elastic stresses such that $J_1 > T$, and $h(t)$ is a heavyside step function. Using this loading in Equation 28, we have $\underline{K} \dot{\underline{\epsilon}} = 0$, and the initial condition $\underline{v}(0) = \underline{K} \underline{\epsilon}^*$, so that the solution for volumetric stresses is:

$$\underline{v}(t) = (\underline{K} \underline{\epsilon}^* - T/3 \underline{m}_T) \exp(-9K_0 \gamma_T t/f_0) + T/3 \underline{m}_T \quad (30)$$

Similarly for Equation 29, we have $\underline{G} \dot{\underline{\epsilon}} = 0$, and the initial condition $\underline{s}(0) = \underline{G} \underline{\epsilon}^*$, so that the solution for deviatoric stresses is:

$$\underline{s}(t) = \underline{G} \underline{\epsilon}^* \exp(-G_0 \gamma_G t/f_0) \quad (31)$$

Some worthwhile observations from these solutions are as follows:

- (1) Since $\underline{\sigma}(t) = \underline{v}(t) + \underline{s}(t)$, the instantaneous elastic stress state is $\underline{\sigma}(0) = \underline{K} \underline{\epsilon}^* + \underline{G} \underline{\epsilon}^* = \underline{D} \underline{\epsilon}^*$
- (2) As time increases, we eventually reach the steady state solution $\underline{v}(\infty) = T/3 \underline{m}_T$ and $\underline{s}(\infty) = 0$, or $\sigma_{11} = \sigma_{22} = \sigma_{33} = T/3$, other $\sigma_{ij} = 0$.
Note, this indeed satisfies the tension-cutoff criterion.

- (3) The exponential rate of stress release from the initial solution to the steady solution is $9K_0\gamma_T/f_0$ for volumetric stresses, and $G_0\gamma_G/f_0$ for deviatoric stresses.
- (4) If it is desired to release volumetric and deviatoric stresses at the same rate controlled by γ_T , we can choose $\gamma_G = \frac{9K_0}{G_0} \gamma_T$.

The exact solution will be used subsequently to validate the numerical solution algorithm presented next.

Numerical Solution Strategy

In the previous work effort (1), a numerical solution algorithm was presented for the viscoplastic cap model without tension cutoff and coded in the program, VPDRVR. Here we extend the algorithm to incorporate the tension-cutoff model. From a programming viewpoint, the incorporation of tension cutoff is straightforward, only requiring modification to the subroutine VPLAST in the VPDRVR program along with the additional input data; T , γ_T and γ_G (see Appendix A).

For completeness, we will review the development of the numerical algorithm along with a flow chart of the complete model wherein the primary objective is to predict the stress response history from a specified strain loading schedule. Alternatively, the VPDRVR program has the option to predict strain history from a stress loading schedule. However, the former option is directly suited for finite element applications.

Numerical Approximation. The basic strategy employs a Crank-Nicolson step-by-step time integration scheme along with a Newton-Raphson iterative solution procedure. We begin with Equation 7 and integrate over one time step, Δt , from time t_n to t_{n+1} to get the incremental constitutive relationship:

$$\underline{\Delta\sigma} = \underline{D}(\underline{\Delta\varepsilon} - \underline{\Delta\varepsilon}_{vp}) \quad (32)$$

where $\underline{\Delta\sigma} = \underline{\sigma}^{n+1} - \underline{\sigma}^n$ with $\underline{\sigma}^n = \underline{\sigma}(t_n)$, similarly for $\underline{\Delta\varepsilon}$ and $\underline{\Delta\varepsilon}_{vp}$.

All quantities at time t_n are presumed known. Next, we approximate $\underline{\Delta\varepsilon}_{vp}$ by a one parameter Crank-Nicolson time integration scheme as:

$$\underline{\Delta\varepsilon}_{vp} = \Delta t((1-\theta)\dot{\underline{\varepsilon}}_{vp}^n + \theta\dot{\underline{\varepsilon}}_{vp}^{n+1}) \quad (33)$$

where θ is the adjustable integration parameter in the range $0 \leq \theta \leq 1$.

Choosing $\theta = 0$ implies the integration scheme is explicit (simple forward difference) so that $\underline{\Delta\varepsilon}_{vp}$ is determined directly from the known value of $\dot{\underline{\varepsilon}}_{vp}^n$ at the beginning of the time step. As a consequence, Δt must be restricted in size to avoid numerical instability (6,7). Alternatively choosing $\theta > 0$, the scheme is implicit since $\underline{\Delta\varepsilon}_{vp}$ is related to the unknown value $\dot{\underline{\varepsilon}}_{vp}^{n+1}$ at the end of the time step; thereby, requiring an iterative solution procedure within the time step. For $\theta \geq 0.5$, the implicit scheme is unconditionally stable so that the choice of Δt is governed by accuracy, not stability.

Algorithm for Strain Loading. Returning to the incremental constitutive relationship with $\underline{\Delta\varepsilon}_{vp}$ replaced by the Crank-Nicolson approximation and using $\underline{\Delta\sigma} = \underline{\sigma}^{n+1} - \underline{\sigma}^n$, we rearrange Equation 32 to get the unknown quantities on the left as:

$$\underline{D}^{-1} \underline{\sigma}^{n+1} + \Delta t \theta \dot{\underline{\varepsilon}}_{vp}^{n+1} = \underline{\Delta\varepsilon} - \Delta t(1-\theta)\dot{\underline{\varepsilon}}_{vp}^n + \underline{D}^{-1} \underline{\sigma}^n \quad (34)$$

Or, more compactly, in a symbolic functional notation.

$$\underline{P}(\underline{\sigma}^{n+1}, \dot{\underline{\varepsilon}}_{vp}^{n+1}) = \underline{q}^n \quad (35)$$

where \underline{P} is the vector of all unknown quantities at time t_{n+1} , and \underline{q}^n is the vector of known quantities including the specified strain increment $\underline{\Delta\varepsilon}$.

For $\theta > 0$, Equation 34 (or Eq. 35) forms a coupled set of six nonlinear algebraic equations for the components of $\underline{\sigma}^{n+1}$ with the understanding that $\dot{\underline{\epsilon}}_{vp}^{n+1}$ is to be replaced by the appropriate flow rule and its associated yield function depending on which region of the cap model is currently being activated (i.e. tension, failure, or cap).

To solve the above, a Newton-Raphson procedure is used by expanding the vector function \underline{p} in a limited Taylor series about a stress state $\underline{\sigma}^i$ which is some estimate of $\underline{\sigma}^{n+1}$, and $\delta\underline{\sigma}^i$ is a first order correction to the estimate, i.e. $\underline{\sigma}^{n+1} = \underline{\sigma}^i + \delta\underline{\sigma}^i$. This leads to a linear set of equations to obtain the correction $\delta\underline{\sigma}^i$ given by:

$$\underline{p}' \delta\underline{\sigma}^i = \underline{q}^n - \underline{p}^i \quad (36)$$

$$\text{where } \underline{p}^i = \underline{D}^{-1} \underline{\sigma}^i + \Delta t \theta \dot{\underline{\epsilon}}_{vp}^i \quad (37)$$

$$\text{and } \underline{p}' = \frac{\partial \underline{p}^i}{\partial \underline{\sigma}} = \underline{D}^{-1} + \Delta t \theta \frac{\partial \dot{\underline{\epsilon}}_{vp}^i}{\partial \underline{\sigma}} \quad (38)$$

Here \underline{p}' is the Jacobian matrix of the vector \underline{p}^i evaluated at $\underline{\sigma}^i, \dot{\underline{\epsilon}}_{vp}^i$.

The iteration process is repeated with $\underline{\sigma}^{i+1} = \underline{\sigma}^i + \delta\underline{\sigma}^i$ to get a new correction $\delta\underline{\sigma}^{i+1}$ until eventually the correction approaches zero. Table 1 summarizes the basic algorithm (Note to start the first iteration ($i=1$), $\underline{p}^i, \underline{p}'^i$, and $\underline{\sigma}^i$ retain their values at time t_n).

Upon reviewing Table 1 it is evident that the updating procedure for $f^{i+1}, \underline{m}^{i+1}, \dot{\underline{\epsilon}}_{vp}^{i+1}$ and \underline{p}'^{i+1} is dependent upon the current value J_1^{i+1} which dictates what region of the model is being activated; tension, failure, or cap. From a computational viewpoint, the updating process can be streamlined by expressing all of the plasticity yield function, f_c, f_f, f_T , and f_G in a general form as:

TABLE 1. Solution algorithm for viscoplastic creep model including tension-cutoff, strain loading.

1. Given at time t_n : $\underline{\epsilon}^n, \underline{\sigma}^n, \underline{\dot{\epsilon}}_{vp}^n, \underline{\dot{\epsilon}}_{vp}^{n-1}, \underline{p}^n, \underline{p}^{n-1}$ and Δt

2. Time loop: $n = 1$ to n_{max}

$$\text{(set)} \quad \underline{g}^n = \Delta t + \Delta t(1 - \theta) \underline{\dot{\epsilon}}_{vp}^n = \underline{\dot{\epsilon}}^{n-1} \Delta t$$

3. Iteration loop: $i = 1, 2, \dots, i_{max}$

$$\text{(solve)} \quad \underline{p}^{i+1} \underline{\sigma}^i = \underline{g}^n - \underline{p}^i$$

$$\text{(update)} \quad \underline{g}^{i+1} = \underline{g}^i + \underline{\sigma}^i$$

$$\underline{\dot{\epsilon}}_{vp}^{i+1} = \underline{\dot{\epsilon}}^{n+1} + \underline{p}^{i+1} \underline{\sigma}^{i+1}$$

$$\underline{f}^{i+1} = \begin{cases} f_T(J_1) + J_1 - 1 & \text{(also compute } f_G) \\ f_T(J_1, J_2) + G - J_2 - 1 \\ f_C(J_1, J_2, \dot{\epsilon}), \quad J_1 = 1 \end{cases}$$

$$\underline{m}^{i+1} = \frac{\partial f}{\partial \underline{\sigma}} \quad \text{(also compute } m_G \text{ if } J_1 = 1)$$

$$\underline{\dot{\epsilon}}_{vp}^{i+1} = \begin{cases} \gamma_T \theta(f_T) m_T + \gamma_G \theta(f_G) m_G, \quad J_1 = 1 \\ \gamma \theta(f) m, \quad J_1 = 1 \end{cases}$$

$$\underline{p}^{i+1} = \underline{Q}^{-1} \underline{g} + \Delta t \theta \underline{\dot{\epsilon}}_{vp}$$

$$\underline{p}^{i+1} = \underline{Q}^{-1} + \gamma \theta \frac{\partial \dot{\epsilon}_{vp}}{\partial \underline{\sigma}}$$

4. Repeat iteration (step 3) unless one of the following is satisfied:

- (a) $\theta = 0$, (explicit integration)
- (b) f^n and $f^{i+1} < 0$, (elastic domain)
- (c) $|\delta \sigma^i| < \text{tolerance}$, (convergence)
- (d) $i > i_{max}$, (iteration limit)

5. Print results and advance to next load increment (Step 2)

6. End

$$f = g_1(J_1, c) = g_2(J_2) \quad (30)$$

where the initial state functions f_1 and f_2 depend on which region of the plasticity surface is active as shown in Fig. 2.

Accordingly, the outward normal vectors, \underline{g}_1 , \underline{g}_2 , \underline{g} , and \underline{g}_0 all have the form

$$\underline{g} = g_1 \underline{b} + g_2 \underline{a} \quad (31)$$

where $g_1 = \partial f_1 / \partial J_1$ and $g_2 = \partial f_2 / \partial J_2$ are explicitly stated in Table 3, and the vectors \underline{b} and \underline{a} are

$$\underline{b} = \frac{\partial J_1}{\partial \underline{x}} = [1, 1, 1, 0, 0, 0]^T \quad (32)$$

$$\underline{a} = \frac{\partial J_2}{\partial \underline{x}} = [g_{11}, g_{22}, g_{33}, g_{12}, g_{13}, g_{23}]^T \quad (33)$$

By carrying out the partial derivatives in Equation 30, the Jacobian matrix can be expressed as

$$P' = \underline{g}'^T = \text{grad}(\underline{g}^T \underline{x}) \cdot \underline{m}^T = \underline{g}'^T \underline{m}^T \quad \text{for } J_1 = c \quad (34)$$

$$\text{or, } P' = \underline{g}'^T = \Delta H \left[\gamma_f \underline{b} + (\gamma_f \underline{m}_f \underline{m}_f^T + \gamma_c \underline{a} \underline{a}^T + \gamma_c \underline{m}_c \underline{m}_c^T + \gamma_c \underline{a} \underline{a}^T) \right] \underline{c} \quad (35)$$

for $J_2 = c$

The first form for \underline{g}' is applicable to the failure or cap surface where it is understood that f and its gradient \underline{g} represents either f_c or f_{cc} and $\underline{g}' = \partial \underline{g} / \partial \underline{x}$. The second form is for the tension cutoff surface where $\underline{g}'_c = \partial \underline{m}_c / \partial \underline{x}$. The viscous flow function θ is common to both forms and only differs by its argument. Thus, $\theta'(f_i)$ is $\partial \theta / \partial f$ evaluated for $f_i = f_1, f_2, f_c$, or f_s .

More conveniently, the Jacobian matrix can be expressed in a common form by using Equation 40 to get:

TABLE 2 Functional forms and parameters for computation

Tension Cutoff $J_1 \leq T$	Failure Surface $C_1 \leq T$	See notes $C_2 \leq T$
$r_1 = \theta_1(J_1)$	$r_2 = \theta_2(J_1) = \theta_2(J_2)$	$r_3 = \theta_3(J_1) = \theta_3(J_2)$
$r_6 = \theta_2(J_2)$		
$q_1 = J_1 - T$	$q_1 = 0 = 1 \text{ exp } \theta_1$	$q_1 = 0 = 1 \text{ exp } \theta_1$
$q'_1 = 1$	$q'_1 = 1 \text{ exp } \theta_1$	$q'_1 = 1 \text{ exp } \theta_1$
$q''_1 = 0$	$q''_1 = 1 \text{ exp } \theta_1$	$q''_1 = 1 \text{ exp } \theta_1$
$\theta_2 = J_2^{1/2}$	$\theta_2 = 1 \text{ exp } \theta_1$	$\theta_2 = 1 \text{ exp } \theta_1$
$\theta'_2 = 1/2 J_2^{-1/2}$	$\theta'_2 = 1 \text{ exp } \theta_1$	$\theta'_2 = 1 \text{ exp } \theta_1$
$\theta''_2 = -1/4 J_2^{-3/2}$	$\theta''_2 = 1 \text{ exp } \theta_1$	$\theta''_2 = 1 \text{ exp } \theta_1$
$x_1 = r_6 \theta_1(r_6) \theta'_1 = \theta(r_6) \theta'_1$	$x_1 = 0 = 1 \text{ exp } \theta_1$	$x_1 = 0 = 1 \text{ exp } \theta_1$
$x_2 = 0.0$	$x_2 = 0 = 1 \text{ exp } \theta_1$	$x_2 = 0 = 1 \text{ exp } \theta_1$
$x_3 = r_1 \theta_1(r_1) \theta'_1$	$x_3 = 0 = 1 \text{ exp } \theta_1$	$x_3 = 0 = 1 \text{ exp } \theta_1$
$x_4 = r_6 \theta_1(r_6) \theta'_1$	$x_4 = 0 = 1 \text{ exp } \theta_1$	$x_4 = 0 = 1 \text{ exp } \theta_1$

$$L = X - R g_1(L) \quad (50)$$

where $g_1(L) = -A + C \exp(BL)$.

For the special hardening rule for soils (not rocks), the same four steps are used when loading the failure or tension surfaces ($J_2 = 1$), except the second step is replaced by

$$\bar{\epsilon}^{i+1} = \min \begin{cases} \bar{\epsilon}^n + \max(0, \Delta \epsilon) \\ \min \{ \exp(BA) \bar{\epsilon}_0, 1 \} \\ 0 \end{cases} \quad (51)$$

where $X_C = J_2 + R g_1(J_2)$ and $\bar{\epsilon}_0$ is the initial value.

This completes the general numerical algorithm for stress loading, however, one last remark is in order. If a nonlinear elasticity relationship is used, i.e., $\dot{\epsilon} = D \dot{\epsilon}_e$ where D is a function of current stress, then the update for $\bar{\epsilon}_{vp}^{i+1}$ in Table I must be done at the incremental level. That is, $\bar{\epsilon}_{vp}^{i+1} = \bar{\epsilon}_{vp}^{n+1} - \bar{\epsilon}_e^{i+1}$ where $\bar{\epsilon}_e^{i+1} = \bar{\epsilon}_e^n + D \bar{\epsilon}_{vp}^{i+1}$. This update procedure is used in the new VPDRVR program and is applicable for both linear and nonlinear forms of the D matrix.

Algorithm for Stress Loading. For the inverse problem, i.e., input stress loading with the objective of determining the strain response, a numerical algorithm similar to that presented in Table I can be easily established. In point of fact the stress loading algorithm is computationally much simpler because the associated Jacobian matrix becomes the identity matrix as illustrated in the following development.

We begin by rewriting Equation 34 with the unknown strain quantities on the left and the known quantities (stress increment and quantities at time t_n) on right to get:

$$\underline{\epsilon}^{n+1} - \Delta t \underline{\sigma} \underline{\epsilon}_{vp}^{n+1} = \underline{D}^{-1} \Delta \underline{\sigma} + \Delta t(1 - \theta) \underline{\epsilon}_{vp}^n + \underline{\epsilon}^n \quad (52)$$

Or, equivalently, in a symbolic functional notation

$$P(\underline{\epsilon}^{n+1}, \underline{\epsilon}_{vp}^{n+1}) = \underline{q}^n \quad (53)$$

where the vectors \underline{P} and \underline{q}^n are the left and right-hand-side of Equation 52, respectively.

For implicit integration ($\nu = 0$), Equation 53 is a set of six nonlinear algebraic equations to be solved by Newton-Raphson iteration.

Alternatively, if explicit integration is used ($\nu = 0$), the equations are linear and do not require iteration.

A Newton-Raphson procedure can be established by expanding \underline{P} in a limited Taylor series about the strain state $\underline{\epsilon}^1$ which is some estimate of $\underline{\epsilon}^{n+1}$, and $\underline{\epsilon}^1$ is a first order correction to the estimate, i.e., $\underline{\epsilon}^{n+1} = \underline{\epsilon}^1 + \delta \underline{\epsilon}^1$. This leads to a linear set of equations for $\underline{\epsilon}^1$ given by

$$\underline{P}' \underline{\epsilon}^1 + \underline{q}^n = \underline{P}^1 \quad (54)$$

where $\underline{P}^1 = \underline{P}(\underline{\epsilon}^1, \underline{\epsilon}_{vp}^1)$ (55)

and $\underline{P}' = \frac{\partial \underline{P}^1}{\partial \underline{\epsilon}} = \underline{I}$ (56)

Here the Jacobian matrix \underline{P}' becomes the identity matrix because $\underline{\epsilon}_{vp}$ can be replaced by the stress dependent flow rule so that $\partial \underline{\epsilon}_{vp} / \partial \underline{\epsilon} = \underline{0}$.

Based on the above, it is evident that the algorithm for stress loading parallels the strain loading algorithm (Table 1) where \underline{P} , \underline{P}' , and \underline{q}^n are replaced by \underline{P} , \underline{P}' , and \underline{q}^n , respectively. Table 3 summarizes the stress loading algorithm. The procedure for updating the hardening parameters \bar{c} , λ , and L is identical for both algorithms.

This completes the algorithm for stress loading.

Discussion of Tension Cutoff Algorithm

In this section we illustrate the performance of the tension cutoff

TABLE 3. Solution algorithm for viscoplastic cap model including tension cutoff (stress loading)

1. Given at time t_n , ϵ^n , J^n , ϵ_{vp}^n , ϵ_{vp}^n , P^n and Δt .

2. Time loop: $n = 1$, to n_{max}

(set) $q^n = D^{-1} \Delta \sigma + \alpha(1 - \nu) \epsilon_{vp}^n + \epsilon^n$

3. Iteration loop: $i = 1, 2, \dots, i_{max}$

(solve) $s_c^i = q^n - P^i$

(update) $\epsilon^{i+1} = \epsilon^i + s_c^i$

$$\epsilon_{vp}^{i+1} = \epsilon^{i+1} - D^{-1} J^{i+1}$$

$$f^{i+1} = \begin{cases} f_T(J_1) & , J_1 > T \quad (\text{also compute } f_G) \\ f_F(J_1, J_2) & , L < J_1 < T \\ f_C(J_1, J_2, i) & , J_1 < L \end{cases}$$

$$m^{i+1} = \frac{\partial f}{\partial \sigma} \quad (\text{also compute } m_G \text{ if } J_1 > T)$$

$$\epsilon_{vp}^{i+1} = \begin{cases} \gamma_T \phi(f_T) m_T + \gamma_G \phi(f_G) m_G & , J_1 > T \\ \gamma \phi(f) m & , J_1 < T \end{cases}$$

$$P^{i+1} = \epsilon^{i+1} - \Delta t \sigma \epsilon_{vp}^{i+1}$$

4. Repeat iteration (step 3) unless one of the following is satisfied:

- (a) $\theta = 0$, (explicit integration)
- (b) f^n and $f^{i+1} < 0$, (elastic domain)
- (c) $|\delta \epsilon^i| < \text{tolerance}$, (convergence)
- (d) $i > i_{max}$, (iteration limit)

5. Print results and advance to next load increment (step 2).

6. End.

algorithm along with an exact solution. Also, a critique of the model is given followed by some suggestions for future improvement.

Illustrative Example. Figure 2a shows a tensile uniaxial strain loading which "abruptly" jumps from 0 to 5% strain and held constant. Also given in the figure are the assumed elastic properties (K_0 and G_0) and the tension cutoff parameters γ_T , γ_G , T and f_0 . Other material properties associated with the failure and cap surfaces are immaterial since only the tension surface is loaded in this example. (For reference, however, the cap and failure surfaces were given the properties for McCormick Ranch Sand (1)). The viscous flow function is chosen as $\phi(f) = f/f_0$ so that the previously developed exact solution (Equation 30 plus Equation 31) can be used as a check.

In this example, the exact solution for axial stress simplifies to:

$$\sigma_{11}(t) = 0.5 \exp(-24t) + 0.1 \quad (\text{ksi}) \quad (57)$$

and lateral stresses ($\sigma_{22} = \sigma_{33}$) are:

$$\sigma_{22}(t) = 0.1 \exp(-24t) + 0.1 \quad (\text{ksi}) \quad (58)$$

These simple forms arise from choosing $\gamma_G = \frac{9K_0}{G_0} \gamma_T$ so that bulk and deviatoric stresses are released at the same rate. From the above equations, it is evident that $\sigma_{11}(0) = 0.6$ ksi and $\sigma_{22}(0) = \sigma_{33}(0) = 0.2$ ksi so that the instantaneous value of $J_1 = 1.0$ ksi indeed triggers tension cutoff ($J_1 = 1.0 > T = 0.3$).

Figure 2b shows the resulting stress histories as obtained from the exact solution and the numerical solution (program VPDRVR). The numerical solution overlaps the exact solution with less than 0.2% error. Most of this small error is due to the finite rise time (0.0001 time units), used

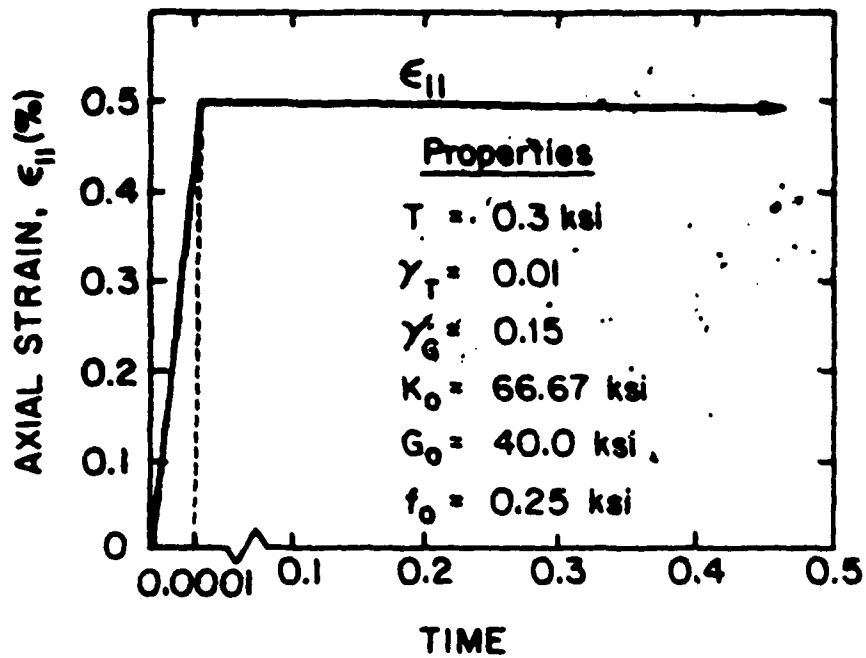


Figure 2a. Uniaxial strain loading for tension cutoff.

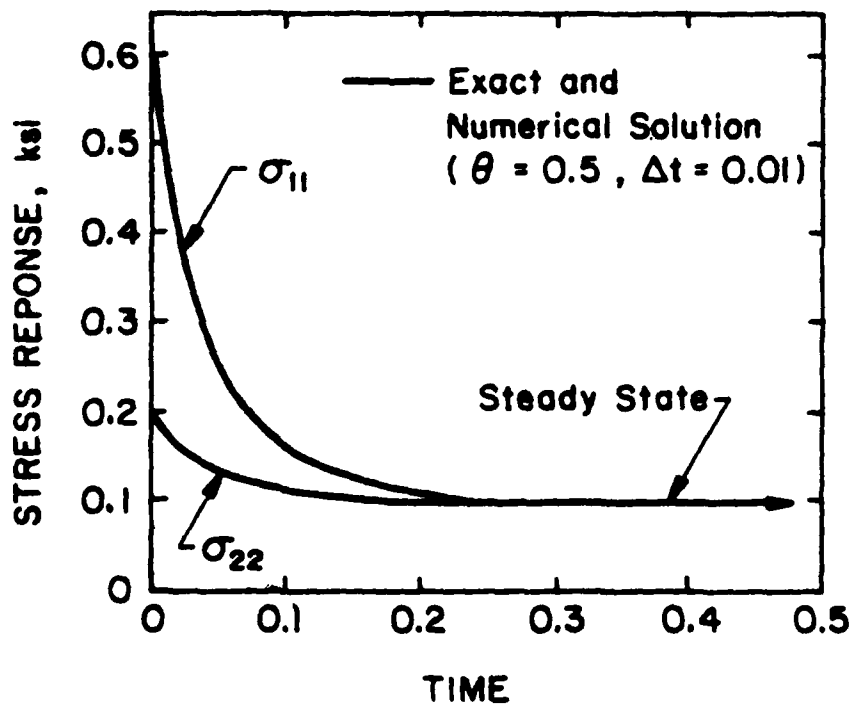


Figure 2b. Stress responses for tension cutoff.

in the numerical solution, as shown in Figure 2a, to simulate a jump loading. It can be observed that the stress responses effectively reach steady state at 0.2 time units after loading ($\sigma_{11} = \sigma_{22} = \sigma_{33} = T/3$). This time period can be increased or decreased by choosing γ_T higher or lower, respectively. It is generally recommended to choose $\gamma_G \geq \frac{9K_0}{G_0} \gamma_T$.

Critique of Tension Cutoff Model. Up till now, little has been said about the rationale of the tension-cutoff criterion, i.e., is it reasonable to assume that hydrostatic tension (J_1) by itself provides an adequate criterion for tension failure. From a rigorous viewpoint, the answer is generally no. However more pragmatically, it depends on the objective of the analysis and, of course, the type of geological material we are dealing with. Granular materials, for example, behave very erratically when one or more of the principal stresses are in tension. In such cases, the J_1 tension criterion may be as appropriate as any other criterion, particularly if the analysis objective is to simply provide a means of effectively reducing the stresses of those elements experiencing tension.

On the other hand, some brittle rock materials exhibit fairly well defined fracture planes when loaded in tension. Here more realistic tension failure theories are available, such as, maximum principal stress theory or William-Warke models (8). These theories employ three independent stress invariants (e.g. J_1 , J_2 and J_3) to describe the initial tension cutoff surface and are inherently anisotropic in the post fracture analysis. When initial tension failure occurs, normal and shear stress components on the fracture plane are released. However on planes orthogonal to the fracture plane, stresses are still active. If additional tensile loading is applied such that three fracture planes develop then all stresses are released and

the effective stiffness in all directions is zero.

To be sure, the J_1 tension cutoff model is not capable of tracking the progressive fracture planes for brittle materials. At best it may be said that J_1 model simulates a complete tension failure with a small residual hydrostatic stress T which may be specified as small as desired.

In summary the J_1 tension model may be adequate for granular materials by default, i.e., other tension cutoff criterion have not demonstrated a faithful representation of granular materials in tension. For brittle materials, the J_1 tension cutoff criterion is a crude approximation, and more rigorous models are available. Nonetheless, if the analysis objective is to simulate loss of material strength in localized areas of tension, the J_1 model provides a good engineering approximation. Many soil-structure problems, including ground-shock problems, fall into this category.

Modifications for Viscoplastic Tension Damage. Presuming that the J_1 tension cutoff criterion is acceptable for some soils and rocks, we now discuss how the viscoplastic tension model could be modified to represent tension damage accumulation. That is, limited experimental evidence indicates that the rate of tensile deformation increases for each loading cycle in tension (9). Conceptually we can conceive of this as the progressive growth of microcracks which do not heal during the cyclic loading.

As previously presented, the viscoplastic tension model is insensitive to tension damage accumulation because regardless of how many times it is cycled into tension, the viscoplastic strain rate $\dot{\epsilon}_{vp}$ remains proportional to the fluidity parameter γ_T and the viscous flow function ϕ (Note γ_G is assumed to be related to γ_T). Thus, if each tension stress cycle is the same, $\dot{\epsilon}_{vp}$ has the same flow rate in each tension cycle.

To simulate the tension damage phenomenon, two modifications are suggested; (1) a strain softening function for the tension cutoff surface, and (2) a functional representation for γ_T . Both functions could employ the same history dependent measure for tension damage accumulation. As an example, the strain softening function for tension could be taken as:

$$f_T(J_1, \bar{\epsilon}_T) = J_1 - T(\bar{\epsilon}_T) \quad (59)$$

$$\text{where } T(\bar{\epsilon}_T) = T_0 \exp(-\alpha_1 \bar{\epsilon}_T) \quad (60)$$

In the above T_0 and α_1 are positive material constants and $\bar{\epsilon}_T$ is a monotonically increasing measure of tension damage accumulation (discussed subsequently). Accordingly, as tension damage accumulates, f_T increases for a given value of J_1 thereby increasing the magnitude of $\dot{\epsilon}_{vp}$. Also, since $T(\bar{\epsilon}_T)$ decreases with increasing tension damage, the tension cutoff criterion is triggered at successively lower values of J_1 in cyclic loading. This mimics non-healing crack growth.

The functional modification for γ_T could be taken as

$$\gamma_T(\bar{\epsilon}_T) = \gamma_{T0} \exp(\alpha_2 \bar{\epsilon}_T) \quad (61)$$

where γ_{T0} and α_2 are positive material constants. Here $\gamma_T(\bar{\epsilon}_T)$ increases with tension damage thereby increasing the viscoplastic strain rate and the rate of stress release.

Lastly, the measure of viscoplastic tension damage accumulation, $\bar{\epsilon}_T$, used in both modifications, could be defined as an accumulation of positive increments of volumetric viscoplastic strain (similar to the cap hardening argument), i.e.,

$$\bar{\epsilon}_T = \bar{\epsilon}_{T0} + \int_0^t \dot{\epsilon}_T dt \quad (62)$$

$$\text{where } \dot{\epsilon}_T = \begin{cases} \dot{\epsilon}_{vp11} + \dot{\epsilon}_{vp22} + \dot{\epsilon}_{vp33}, & f_T > 0 \\ 0, & f_T < 0 \end{cases} \quad (63)$$

and $\bar{\epsilon}_{T0}$ is an initial value for tension damage.

The foregoing modifications are merely suggestions to indicate how viscoplastic tension damage accumulation could be represented within the general framework of the viscoplastic cap model. Although the incorporation of these modifications into a computational procedure is relatively straightforward, more experimental data is needed to verify the validity of these or other possible forms.

PART II. PARAMETER IDENTIFICATION AND EXAMPLES

Introduction

The complete description of the viscoplastic cap model requires the following identifications; elastic parameters (K and G), failure surface parameters (A, B, and C), cap surface parameters (X_0 and R) along with hardening parameters (W and D), tension cutoff parameter (T), and the viscous flow function exponent (N) along with the compressive fluidity parameter (γ) and the tensile fluidity parameters (γ_T and γ_G). The normalizing constant (f_0) should not be viewed as an independent parameter and is recommended to be taken as $f_0 = A$.

For subsequence reference, the pertinent functional forms employing the above parameters are listed below (excluding tension cutoff).

Failure and cap surfaces.

$$f = \begin{cases} f_F = \sqrt{J_1} - (A - C \exp(BJ_1)) , & T > J_1 > L \\ f_C = (J_1^2 - ((X - L)^2 - (J_1 - L)^2)/R^2)/f_0 , & J_1 < L \end{cases} \quad (64)$$

$$(65)$$

Cap hardening.

$$X = \ln(\bar{\epsilon}/W + 1)/D \quad (66)$$

$$\bar{\epsilon} = \bar{\epsilon}_0 + \int_0^t \dot{\bar{\epsilon}} dt \quad (67)$$

$$\dot{\bar{\epsilon}} = \begin{cases} \min(\dot{\omega}_{vp}, 0) , & J_1 < L \\ \max(\dot{\omega}_{vp}, 0) , & J_1 > L \quad (\text{soil only}) \end{cases} \quad (68)$$

$$\dot{\omega}_{vp} = \dot{\epsilon}_{vp11} + \dot{\epsilon}_{vp22} + \dot{\epsilon}_{vp33} \quad (69)$$

$$\bar{\epsilon}_0 = W(\exp(DX_0) - 1) \quad (70)$$

$$L = X + R(A - C \exp(BL)) \quad (71)$$

Viscous flow rule.

$$\dot{\epsilon}_{vp} = \gamma \phi(f) \underline{m} \quad (72)$$

$$\phi(f) = \begin{cases} (f/f_0)^N, & f > 0 \\ 0, & f \leq 0 \end{cases} \quad (73)$$

$$\underline{m} = \frac{\partial f}{\partial \underline{\sigma}} = g'_1 \underline{b} + g'_2 \underline{a} \quad (74)$$

Constitutive relationship.

$$\dot{\underline{\sigma}} = \underline{D} \dot{\underline{\epsilon}}_e \quad (75)$$

$$\dot{\underline{\epsilon}}_e = \dot{\underline{\epsilon}} - \dot{\underline{\epsilon}}_{vp} \quad (76)$$

All the above forms have been developed and discussed in the first part of this report as well as in Reference (1). The tension cutoff equations are not repeated here since the identification of the associated parameters (T , γ_T and γ_G) has already been addressed, i.e., T should be selected as some fraction of FCUT (say $T = 0.5$ FCUT), and $\gamma_G = 9K \gamma_T/G$, and γ_T taken an order of magnitude larger than γ .

We now consider identification techniques for the remaining parameters. To be sure, identification is a difficult, non-unique process and is dependent upon the quality and quantity of experimental data. With regard to identification, experimental testing may be grouped in two categories "ideal" experiments and "non-ideal" experiments. The former is a complete set of experiments explicitly designed to provide relatively easy parameter identification by controlling the loading schedule to permit separate identification of viscous and plastic (steady-state) responses. Conversely,

the "non-ideal" experiments are incomplete and/or do not provide direct information on uncoupling viscous and plastic (steady-state) responses. For the non-ideal cases, parameter identification is probably best achieved by a trial and error approach using the VPDRVR program.

Parameter identification for both the ideal and non-ideal cases is discussed in subsequent sections. Unfortunately most of the existing experimental data for soil and rocks falls into the "non-ideal" category. To circumvent this problem, we will define an ideal set of experiments along with a hypothetical set of results to illustrate the "ideal" identification procedures. Hopefully this will serve as a template for future experimental work. For the non-ideal cases, existing experimental data will be used to illustrate parameter identification by a trial and error process using the VPDRVR program.

Before these identification procedures are presented, it is well to discuss some behavioral aspects of the viscoplastic cap model along with the influence that various parameters have on the model's response.

Model Behavior and Parameter Influence

The behavior of the viscoplastic cap model is best visualized by considering the plasticity surfaces in $J_1, \sqrt{J_2}$ space as shown in Figure 3a. Here the initial cap setting, X_0 , defines the initial elastic region shown by the shaded area. To begin with, we suppose a compressive stress state " σ_A " is suddenly applied and held constant such that $f_c(\sigma_A, X_0) > 0$ but within the failure surface as illustrated in Fig. 3a. Viscoplastic flow will commence with a rate proportional to $\gamma \phi(f_c) \underline{m}$, Eq. 72. At the same time, the cap location X will begin to move from its initial location X_0 toward the location X_A so that as time passes $f_c(\sigma_A, X)$ (and hence $\dot{\epsilon}_{vp}$)

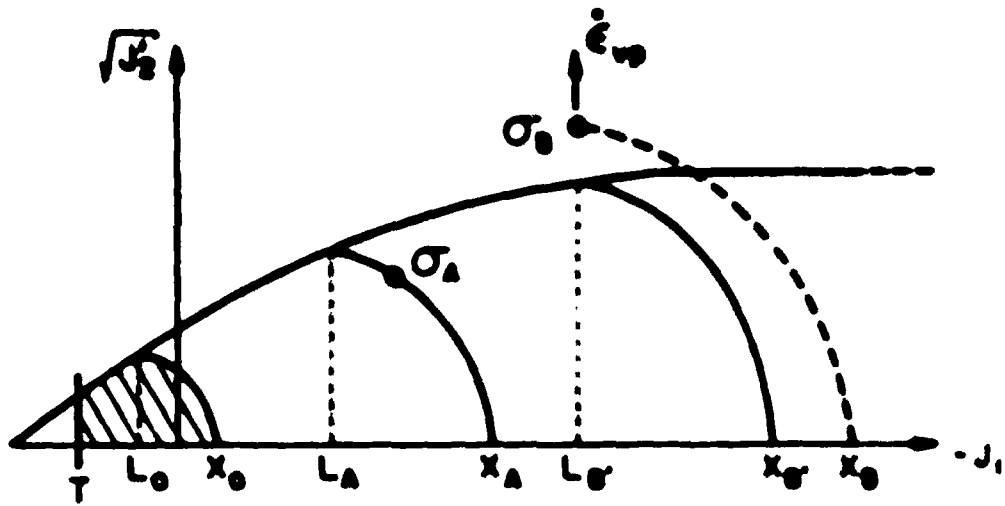


Figure 3a. Illustration of cap movement and steady-state conditions.

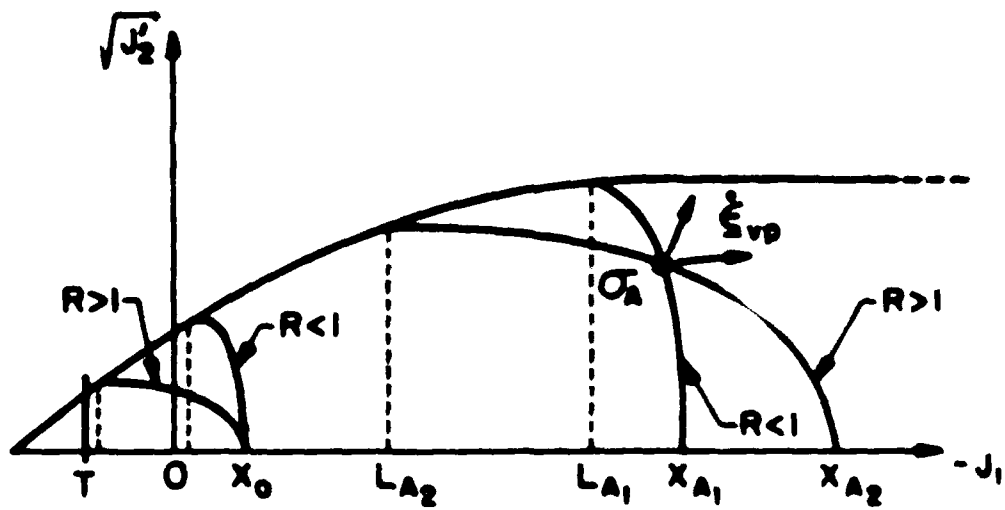


Figure 3b. Influence of parameter R on viscoplastic strains.

approaches zero. The length of time it takes for $\dot{\epsilon}$ to reach $\dot{\epsilon}_f$ is dependent on the hardening function, $\dot{\epsilon}_f$ is which is both dependent on the accumulated viscoplastic volumetric strain, ϵ_v , and on the history of the hysteretic of the hardening rate taken. For time $t > t_f$, observe that, eventually when $\dot{\epsilon} = \dot{\epsilon}_f$, we have the steady state condition $\dot{\epsilon}_{ij} = 0$ because $\dot{\epsilon}_{ij}(\dot{\epsilon}_f, \dot{\epsilon}_f) = 0$. At steady state conditions, the viscoplastic strains ϵ_{ij} would be identical to the plastic strains obtained from a corresponding viscoplastic model.

Next we consider a sudden increase in stress from σ_1 to σ_2 such that $\dot{\epsilon}_{ij}(\sigma_2, \dot{\epsilon}_f) = 0$ and σ_2 lies outside the failure surface as shown in Fig. 1a. As before, $\dot{\epsilon}$ begins to move from $\dot{\epsilon}_1$ to location $\dot{\epsilon}_2$ on $\dot{\epsilon}_f$ where $\dot{\epsilon}_{ij}(\sigma_2, \dot{\epsilon}_2) = 0$. However in this case, $\dot{\epsilon}$ never reaches $\dot{\epsilon}_2$ but rather $\dot{\epsilon}$ stops moving at the location $\dot{\epsilon}_3$ on $\dot{\epsilon}_f$ where $\dot{\epsilon}_3 = \dot{\epsilon}_2$. The reason that $\dot{\epsilon}$ remains stationary at $\dot{\epsilon}_3$ is because at this cap location $\dot{\epsilon}_3$ has no components in the volumetric direction so that $\dot{\epsilon}_{ij} = \dot{\epsilon}_{ij} = 0$ (see Fig. 2a). Hence, $\dot{\epsilon}$ remains constant according to the hardening function, equation 6d. As a consequence, we have a steady-state "failure" condition in which deviatoric viscoplastic strains continue to increase at a constant rate proportional to the excess deviatoric stresses above the failure surface. These behavioral characteristics will be taken advantage of in subsequent identification procedures.

Perhaps the most elusive parameters of all the viscoplastic cap model parameters are R , W and β which are associated with cap surface. We begin by considering the parameter β which controls the cap shape. $\beta = 1$, $\beta = 1$, or $\beta = 1$, inferring the shape is a vertical ellipse, circle, or horizontal ellipse, respectively. Figure 3b illustrates two cap shapes, $\beta = 1$ and $\beta = 1$ plotted on the same graph, it is assumed all other parameters are common

to both model shapes. As before if a stress state σ_A is suddenly imposed, both cap surfaces will move from their initial locations and eventually reach a steady-state position containing the stress-state σ_A as shown. During this movement, the relative distribution of volumetric and deviatoric viscoplastic strains is governed by the outward normal at σ_A . Consequently the vertical ellipse ($R = 1$) distributes a greater proportion of its viscoplastic strain to the volumetric components than does the horizontal ellipse ($R = 1$). Thus, the major purpose of the parameter R is to control the relative distribution of volumetric and deviatoric viscoplastic strain components.

Cap hardening, which locates the current position of A , employs the parameters W and D along with the accumulated viscoplastic strain hardening measure $\bar{\epsilon}$ as given by Equation 66. However the influence of W and D is much more complicated than this equation initially suggests because ultimately $\bar{\epsilon}$ is also dependent on W and D through the viscoplastic flow rule. Nonetheless, if Equation 66 is plotted in nondimensional form as shown in Figure 4, it can be used to great advantage in understanding the hardening behavior, as well as, helping to quantify the W and D parameters.

Listed below are some useful insights with regard to the hardening relationships in Figure 4.

- (1) D (units of inverse stress) and W (units of strain) are positive constants so that $D\bar{\epsilon}$ and $\bar{\epsilon}/W$ are dimensionless hardening coordinates. At any instant in time $D\bar{\epsilon}$ and $\bar{\epsilon}/W$ are related by the graph in Figure 4.
- (2) Assuming the initial value of $X = X_0$ is negative (which also gives $\bar{\epsilon}_0 < 0$) then all subsequent values of X and $\bar{\epsilon}$ are negative such that $X_0 \geq X \geq -\infty$ and $\bar{\epsilon}_0 \geq \bar{\epsilon} \geq -W$. Thus W represents the maximum

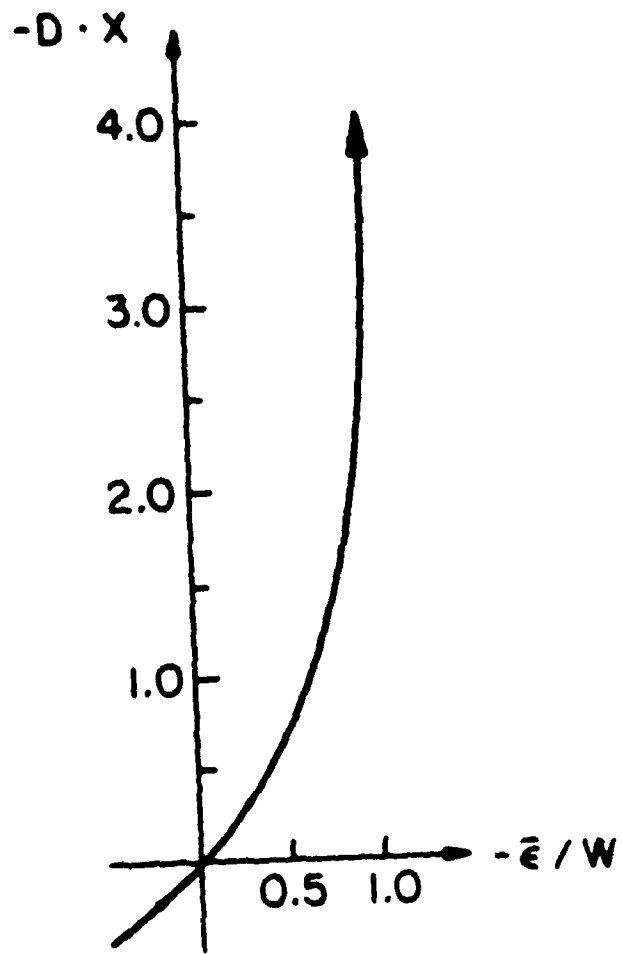


Figure 4. Relationship between hardening parameters W and D .

absolute value of volumetric viscoplastic strain accumulation that can ever be achieved under any loading.

- (3) When $\bar{\epsilon}/W \rightarrow -1.0$ or, equivalently, when $|DX| > 3.0$ (approximately) we see that a small change in $\Delta\bar{\epsilon} = \dot{\bar{\epsilon}}\Delta t$ produces a large change $\Delta X = \dot{X}\Delta t$. As a consequence X moves its position (hardens) very rapidly toward the steady-state position so that the net response is almost entirely elastic (i.e., there is no time for viscoplastic strains to accumulate). This is why the cap model produces an asymptotically increasing stress-strain curve in hydrostatic compression, in effect, a pure elastic slope in the limit.

Based on the above insights, experience has shown that it is usually best to quantify the parameter D in conjunction with X_0 . That is, X_0 is first chosen to establish the size of the initial elastic domain, then D is chosen such that $|DX_0| < 3.0$ in order that plastic hardening will be effective. Typically $|DX_0| \leq 0.5$ has been used in this study. Having made the selection for D , the parameter W may be used for control. Increasing W results in increased amounts of viscoplastic strain, and conversely, decreasing W decreases the amount of viscoplastic straining.

Identification Guidelines

Summarized below are the behavioral aspects and parameter identification guidelines for the viscoplastic cap model.

Elastic Parameters. The bulk modulus K and shear modulus G control the elastic response. These parameters are best determined from unloading tests and are restricted such that $K \geq 2/3G$. Nonlinear forms, $K = K(J_1)$ and $G = G(J_2)$, may be used if warranted.

Failure Surface. The failure surface, denoted by f_f in Equation 64, is

defined by parameters A, B, and C and forms a static yield surface $f_f = 0$ along which the cap surface can move. If a constant stress state is imposed such that $f_f > 0$, steady-state failure conditions will result wherein the deviatoric components of $\underline{\epsilon}_{vp}$ will continue to increase at a constant rate. The parameter A is the maximum height of the static failure surface and A-C is the height at $J_1 = 0$, hence $A > C$. The parameter B controls the curvature of the static yield surface, as B increases, the rate of curvature increases.

Cap Surface. The cap surface, denoted by f_c in Equation 65, is an ellipse quadrant whose shape is governed by the parameter R and whose initial location is set by χ_0 . Choosing $R > 1$ implies a horizontal ellipse whereas $R < 1$ implies a vertical ellipse. By increasing R the outward normal of the cap surface leans more toward the deviatoric direction ($\sqrt{J'_2}$) so that a greater proportion of $\dot{\underline{\epsilon}}_{vp}$ is weighted toward the deviatoric components as opposed to the volumetric components. In a typical triaxial stress loading, for example, the effect of increasing R is to increase the total axial strain ϵ_{11} . As a first guess, use $R = 1.0$ for trial and error identification.

Setting χ_0 to a large negative value provides a large initial elastic space which is often a suitable representation for pre-consolidated soils or rocks. However remolded soil specimens are usually best represented with an initially small elastic domain in which case χ_0 is assigned a small negative value near the J_1 origin. Once χ_0 is selected, $\bar{\epsilon}_0$ is given by Equation 70, and L_0 is given by Equation 71.

Cap Hardening. The parameters D and W, Equation 66, control cap hardening along with the accumulated volumetric viscoplastic strain measure $\bar{\epsilon}$, Equations 67-70. Experience has shown it is best to set $D \leq 1/2 |\chi_0|^{-1}$

and use W to control the cap hardening. To wit, increasing W retards the cap movement thereby increasing the accumulation of ϵ_{vp} . As $|\bar{\epsilon}/W|$ approaches 1.0, the rate of cap movement X becomes infinite, and hence, the response becomes more elastic.

Viscous Parameters. The cap/failure fluidity parameter γ linearly controls the viscoplastic strain rate $\dot{\epsilon}_{vp}$ via Equation 72. The exponent N also influences the rate but in a nonlinear fashion dependent on the current value of f/f_0 , i.e. $\dot{\epsilon}_{vp} = \gamma \phi(f/f_0)^N$. Typically $N = 1$ is used, and $\dot{\epsilon}_{vp}$ is controlled by γ unless sufficient experimental data is available to quantify both parameters. The tension fluidity parameters are usually chosen on an arbitrary basis since experimental data in tension is usually lacking. It is recommended to choose γ_T an order of magnitude larger than γ and set $\gamma_G = 9 K/G \gamma_T$.

Tension Cutoff. The tension cutoff parameter T is also usually chosen on an arbitrary basis. However, it is limited to a small practical range, $0 \leq T \leq FCUT$, where $FCUT$ is the intersection of the failure surface with the J_1 axis. Typically, we set $T = FCUT/2$, but we must check that $T \geq L_0$ if L_0 is positive.

The foregoing guidelines are used extensively in the following identification procedures.

Parameter Identification Using Ideal Experimental Data

In the following, an ideal experiment is defined and hypothetical results are constructed to illustrate an identification procedure.

Loading Schedules. A conventional triaxial testing apparatus is used to conduct the ideal test. We require at least one purely hydrostatic test and a minimum of three triaxial tests with successively increased confining pressures. Figure 5a illustrates the stress paths of these tests in terms

of σ_1 and σ_3 where H is the hydrostatic test ($\sigma_1 = \sigma_3$) and T_1, T_2, T_3 are the triaxial tests. Each test employs a virgin material specimen, and as illustrated, we require an unload-reload cycle on the hydrostatic test and one of the triaxial tests.

The time loading schedule for the hydrostatic tests is illustrated in Figure 5b. Here a sequence of pressure increments are applied such that each increment is maintained until steady-state conditions are observed (i.e. no volume change, $\dot{w} = 0$). Similarly, the time loading schedule for each triaxial test is a sequence of axial stress increments as shown in Figure 5c. To start, we require the initial hydrostatic loading to be at a steady-state condition before the first axial load increment is applied. Each axial load increment is applied and held constant until a steady-state condition $\dot{\epsilon}_1 = 0$ is observed for axial strain after which the next load increment is applied. Eventually a failure condition is observed $\dot{\epsilon}_1 =$ constant (or increasing in rate) which terminates the test. In both types of tests an unload-reload cycle is conducted from a steady-state position.

Response Data. For the hydrostatic test we require steady-state data of pressure vs. volumetric change, as well as, a time history plot of volumetric change vs. time. For each triaxial test we require steady-state data of shear stress $\sigma_1 - \sigma_3$ vs. axial and lateral strains. As the first step in parameter identification, we will use steady-state data to identify the plasticity parameters. To this end, the hypothetical stress-strain responses are plotted in Figures 6a and 6b.

Identification Procedure. The basic strategy for parameter identification is to determine elastic parameters from unloading data, plasticity parameters from steady-state data, and viscous parameters from time history response data. This is illustrated in the following steps.

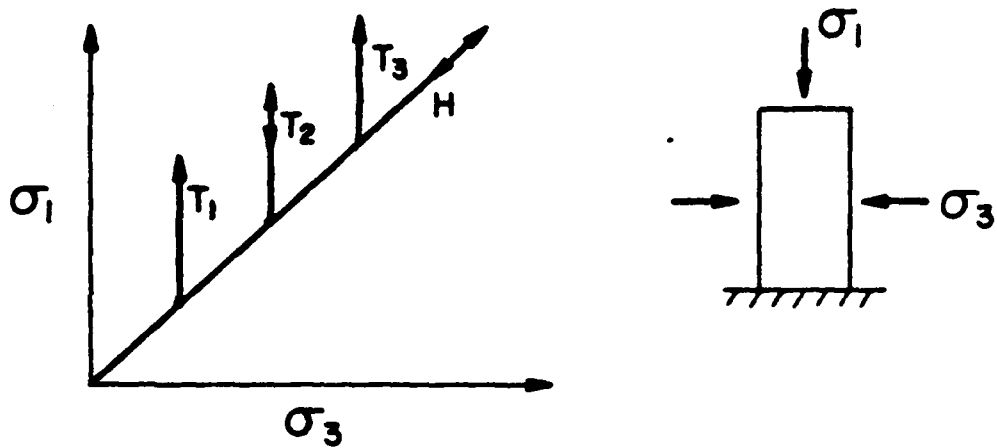


Figure 5a. Stress path loadings, triaxial and hydrostatic.

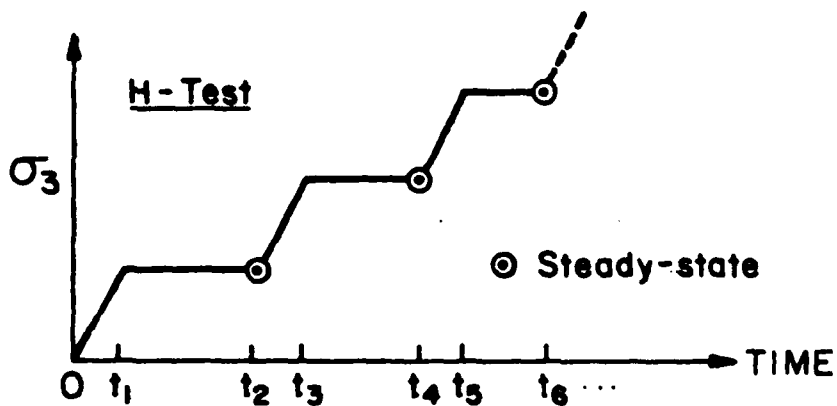


Figure 5b. Hydrostatic test loading schedule.

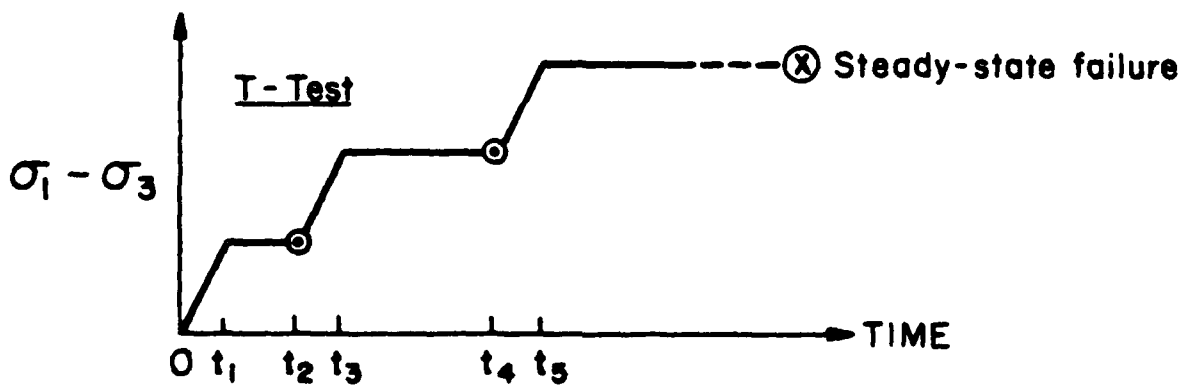


Figure 5c. Triaxial test loading schedule.

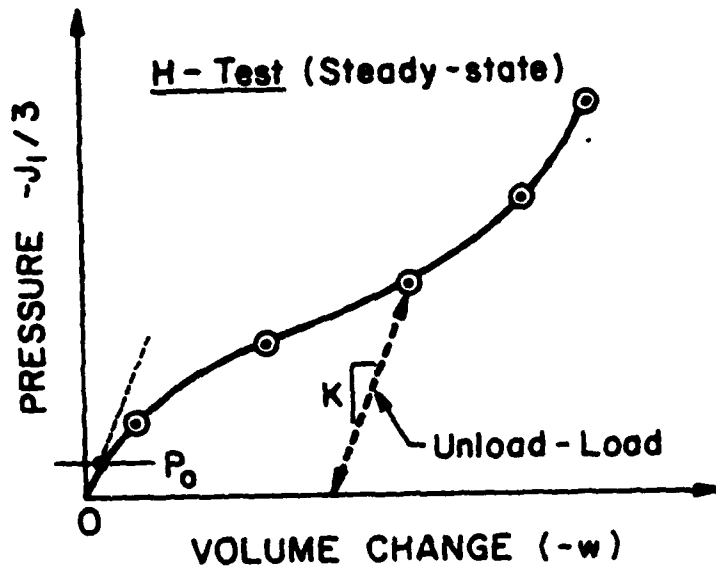


Figure 6a. Pressure vs. volume change at steady states.

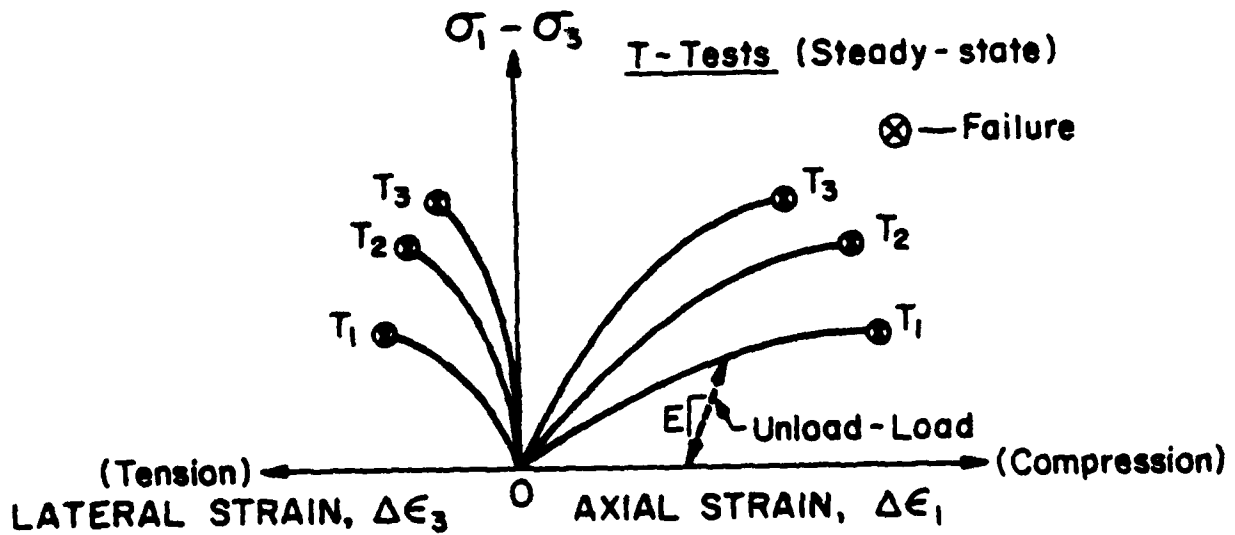


Figure 6b. Shear stress vs. axial and lateral strain at steady states.

- (1) Elastic parameters (K, G). The bulk modulus K is the slope of the hydrostatic unload-load curve (Figure 6a) and Young's modulus is the slope of the triaxial unload-load curve (Figure 6b). Thus, $G = 3KE/(9K-E)$.
- (2) Initial elastic domain (X_0). The initial elastic domain as controlled by X_0 can be determined by transferring the bulk modulus slope K to the origin of Figure 6a and finding the pressure P_0 at which the slope departs from the data curve. Thus, $X_0 = 3P_0$.
- (3) Failure surface (A,B,C). The failure points for tests T_1 , T_2 , and T_3 (Figure 6b) represent the maximum steady-state shear stress obtainable for each confining pressure. These three points may be plotted in $J_1, \sqrt{J'_2}$ space with $J_1 = \sigma_1 + 2\sigma_3$ and $\sqrt{J'_2} = |\sigma_1 - \sigma_3|/\sqrt{3}$ as shown in Figure 7. Accordingly, the parameters A, B, and C may be determined by the failure condition $f_F = 0$, (i.e., $\sqrt{J'_2} = A - C \exp(BJ_1)$) for the three data points. This may be done graphically by establishing the values for A and C as shown in Figure 7 and using the above equation to compute B. Alternatively, a least-squares error fit could be used to get A, B, and C simultaneously.
- (4) Cap hardening (W, D). Since hardening is controlled by the volumetric viscoplastic strain measure $\bar{\epsilon}$, the steady state hydrostatic data (Figure 6a) is sufficient to determine the hardening parameters W and D by using Equation 66. To this end, we note that the steady-state hydrostatic data implies $X = J_1$ (i.e., X coincides with J_1 at steady-state) and $\bar{\epsilon} = \epsilon_0 + w_{vp}$ (i.e., w_{vp} is always compressive so that all increments add to $\bar{\epsilon}$). Since $w_{vp} = w - J_1/3K$ we can say $\bar{\epsilon} = \bar{\epsilon}_0 + w - J_1/3K$, where $\bar{\epsilon}_0$ is defined by Equation 70. Substituting the above relationships for X, $\bar{\epsilon}$ and $\bar{\epsilon}_0$ into Equation

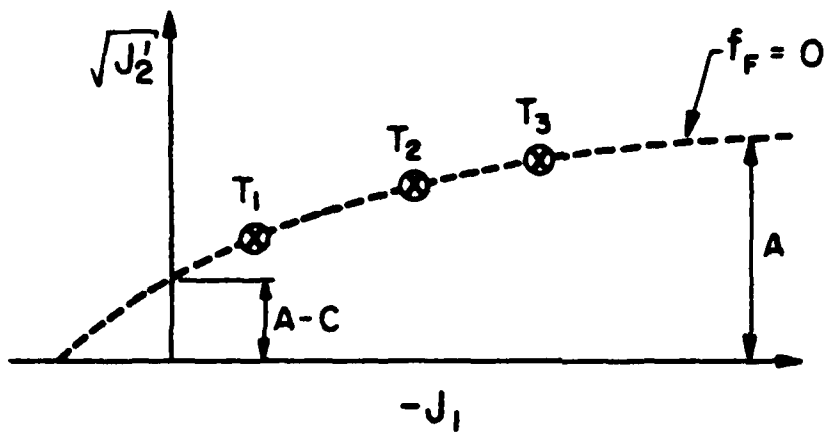


Figure 7. Failure surface plot.

66 we have

$$W(\exp(DJ_1) - \exp(DX_0)) = w - J_1/3K$$

In the above K and X_0 are known constants (Steps 1 and 2) and w and J_1 are steady-state data points in Figure 6a. Accordingly, the unknown parameters W and D are to be determined to best satisfy the above equation for all data points. The easiest way to do this is to choose $D \approx 1/2 |X_0|^{-1}$ and directly solve for W at several (J_1, w) data points. If each of the W 's so determined is not approximately the same, make a small adjustment in D and try again.

- (5) Cap shape (R). The strategy to determine R is illustrated in Figure 8 where a particular failure data point (T_2) is chosen with known coordinates $J_1^*, \sqrt{J_2^*}$. At this point, we have $L = J_1^*$, and our objective is to determine the location X so that R is given by $R = (L - X)/\sqrt{J_2^*}$. To get X we use the hardening function, Equation 66, in which W and D have already been determined, so our problem is to find $\bar{\epsilon}$ at the failure point $J_1^*, \sqrt{J_2^*}$. This may be achieved by adding the volumetric viscoplastic strain from the hydrostatic test evaluated at J_1^* with the additional volumetric viscoplastic strains from triaxial test T_2 (Figure 6b). Thus the computational steps are as follows:

$$w = w(J_1^*) + (\Delta\epsilon_1 + 2\Delta\epsilon_3) \quad \text{(volumetric strain)}$$

$$w_{vp} = w - J_1^*/3K \quad \text{(viscoplastic volumetric strain)}$$

$$\bar{\epsilon} = \epsilon_0 + w_{vp} \quad \text{(hardening strain)}$$

$$X = \ln(\bar{\epsilon}/W + 1)/D \quad \text{(cap X associated with } J_1^*, J_2^*)$$

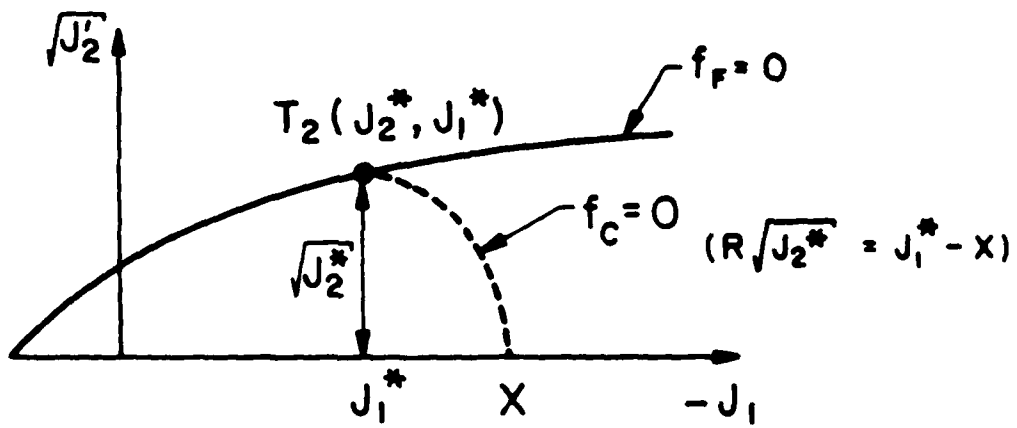


Figure 8. Cap surface plot for determining R.

$$R = (J_1^* - X) / \nu_0^* \quad \text{Determination of } \nu$$

This process may be repeated for as many failure points (J_1^*, ν_0^*) as desired and an average value of ν can be determined.

- (6) Viscous Parameters γ, N . Using non-steady-state data the parameters γ and N can be determined from the hydrostatic test by matching viscoplastic volumetric strain rate data with the viscoplastic flow rule, equation 66. To begin with, we plot w_{vp} vs. time as illustrated in figure 9 where the time stations t_1, t_2 , etc. correspond to the hydrostatic loading schedule in figure 5b. At the beginning of each creep phase, e.g., time = t_1 in figure 9, the volumetric viscoplastic strain rate $w_{vp}(t_1)$ can be measured as the tangent to the time history plot. Such data values $w_{vp}(t_j)$ may be obtained for each time station $t_1, t_2, t_3, t_5, \dots$ terminating a load increase. Equating this data to the volumetric viscoplastic flow rule we have

$$\dot{w}_{vp}(t_j) = \frac{1}{\gamma} f_c \left(\frac{J_1(t_j) - L(t_j)}{f_0} \right)^N (3m_j)$$

where $m_j = 2(J_1(t_j) - L(t_j)) / f_0 \nu^2$

It is understood that f_c and m_j are to be evaluated at time t_j . Evaluating f_c and m_j is laborious but straightforward as follows, first compute $\dot{\epsilon}(t_j) = \dot{\epsilon}_0 + w_{vp}(t_j)$, second compute $\lambda(t_j)$ from Equation 66, and third compute $L(t_j)$ from Equation 71. Having λ and L along with $J_1(t_j)$, f_c and m_j may be directly evaluated since all plasticity parameters are known and $J_1' = 0$.

Now for each $w_{vp}(t_j)$ data point everything is known in the above expression except γ and N . These parameters can be determined by a least-square error technique. Or, more simply, choose

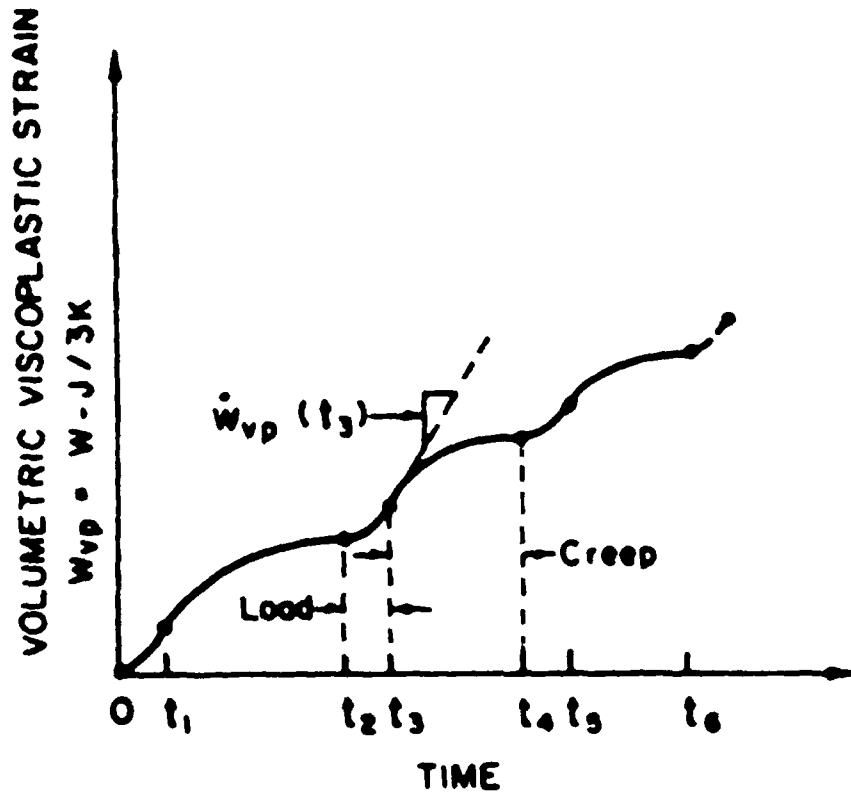


Figure 9. Volumetric viscoplastic strain history plot to determine viscous parameters

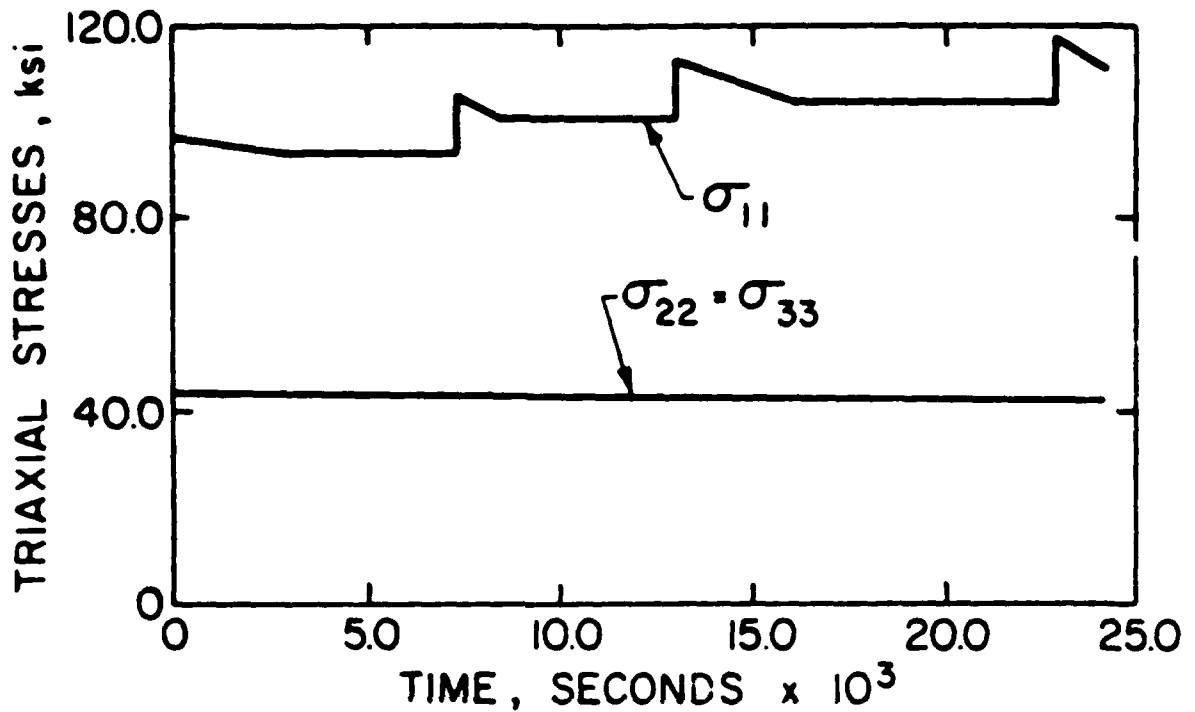
$N = 1$ and determine values of α and β . If the computed fits are not in good agreement adjust N and try again.

This completes the ideal identification process, we next consider trial and error methods with the VPDRVR program.

Parameter Identification Using Non-Ideal Experimental Data

Three distinct sets of experimental are considered for the purpose of identifying the viscoplastic parameters by a trial and error procedure using the VPDRVR program. The three experiments represent a range of geological materials, hard limestone, soft sedimentary rock, and well-graded sand. Further, the manner of loading and loading rates are significantly different between each experiment, thus, this study not only illustrates the parameter identification process, but also, demonstrates the capabilities and limitations of the viscoplastic cap model. Each experiment and corresponding parameter fit is discussed in turn.

Limestone in Triaxial Stress. A rather elaborate, nonstandard, triaxial test experiment on specimens of Solenhofen Limestone was conducted by Robertson (10) to measure the axial strain history ϵ_{11} resulting from a variable axial stress loading sequence. Details of the testing apparatus and experimental program are somewhat involved and are not repeated here. Instead, we simply identify the stress loading history (Figure 10) for Robertson's specimen number S-90 which is considered in this study. As shown in Figure 10, an initial triaxial stress state is rapidly imposed ($\sigma_{11} = 96.1$ ksi, $\sigma_{22} = \sigma_{33} = 44.1$ ksi). Thereafter, the lateral stresses are maintained constant, and the axial stress is intermittently step loaded at time = 7.2, 12.9, and 22.8 kiloseconds. After each step loading including the initial loading, σ_{11} decreases by some amount due to the nature of the



MODEL PARAMETERS FOR LIMESTONE

Elastic Moduli: Bulk = 3,500 ksi ; shear, $G(J_2') = 91 (1 + 21 \exp(-0.0012 J_2'))$ ksi

Failure Surface: $f_F(J_1, J_2') = \sqrt{J_2'} - (1.0 - 0.25 J_1)$ ksi

Cap Surface: $R = 2.4$; $f_0 = 1.0$ ksi ; $X_0 = -212.0$ ksi

Cap Hardening: $W = 0.55$; $D_0 = 0.0024$ ksi⁻¹

Viscous Flow Function:

$N = 1$; $f_0 = 1.0$ ksi

$\gamma = 0.2 \times 10^9$ sec⁻¹

Figure 10. Triaxial stress loading schedule and model parameters for limestone.

hydraulic testing apparatus. Although the magnitude of these decreases were reported, their time history was not. Accordingly, the linearly decreasing functions following each jump in Figure 10 are approximations.

Axial strain measurements were recorded before and after each loading step, providing a data base for attempting to "curve fit" the viscoplastic cap model. Since the experiment represents a consecutive sequence of loadings, "curve fitting", in this case, is quite difficult because the accumulated strain depends upon the entire loading history and the strain hardening parameter $\bar{\epsilon}$ controlling the cap movement.

Figure 11 shows strain history data points along with a viscoplastic cap model representation producing a fairly good correlation. Since the viscoplastic model was driven by the triaxial stress loading schedule in Figure 10, the stress loading algorithm was used in the VPDRVR program. The final parameters for the viscoplastic cap model are also shown in Figure 10 and were largely determined by trial and error, discussed next.

Isotropic elastic parameters, bulk modulus and shear modulus, were determined by best fitting the instantaneous jump responses, i.e., no viscoplastic flow was assumed to occur during the loading jumps. This was best matched by a constant bulk modulus and a variable shear modulus monotonically decreasing with J'_2 (Fig. 10). The failure surface was simplified to a standard Drucker-Prager form and the initial cap surface, shaped as a horizontal ellipse $R = 2.4$, was located well into the compression region by setting $X_0 = -212.0$ ksi. The motivation for this initial setting was to provide a large elastic region so that the initial jump loading did not cause excessive viscoplastic flow in accordance with observations. Also it insured the viscoplastic flow in accordance with the cap surface ($J_1 \leq L$) throughout the loading schedule.

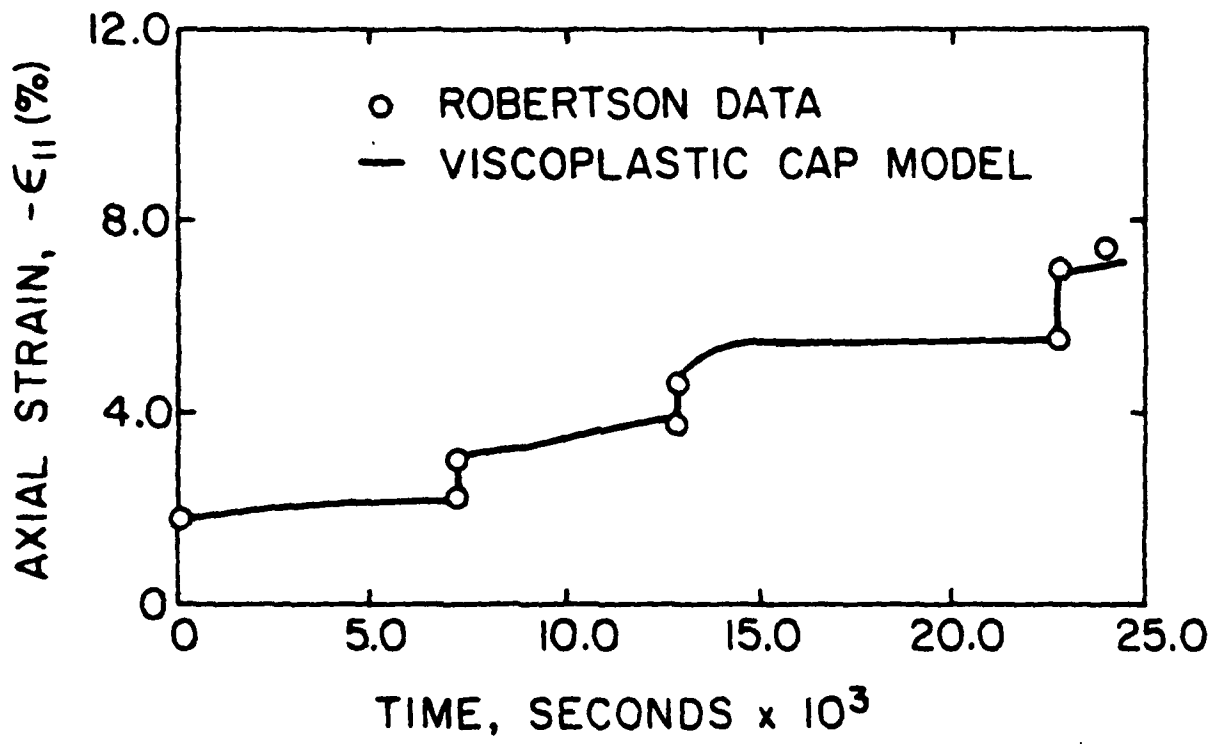


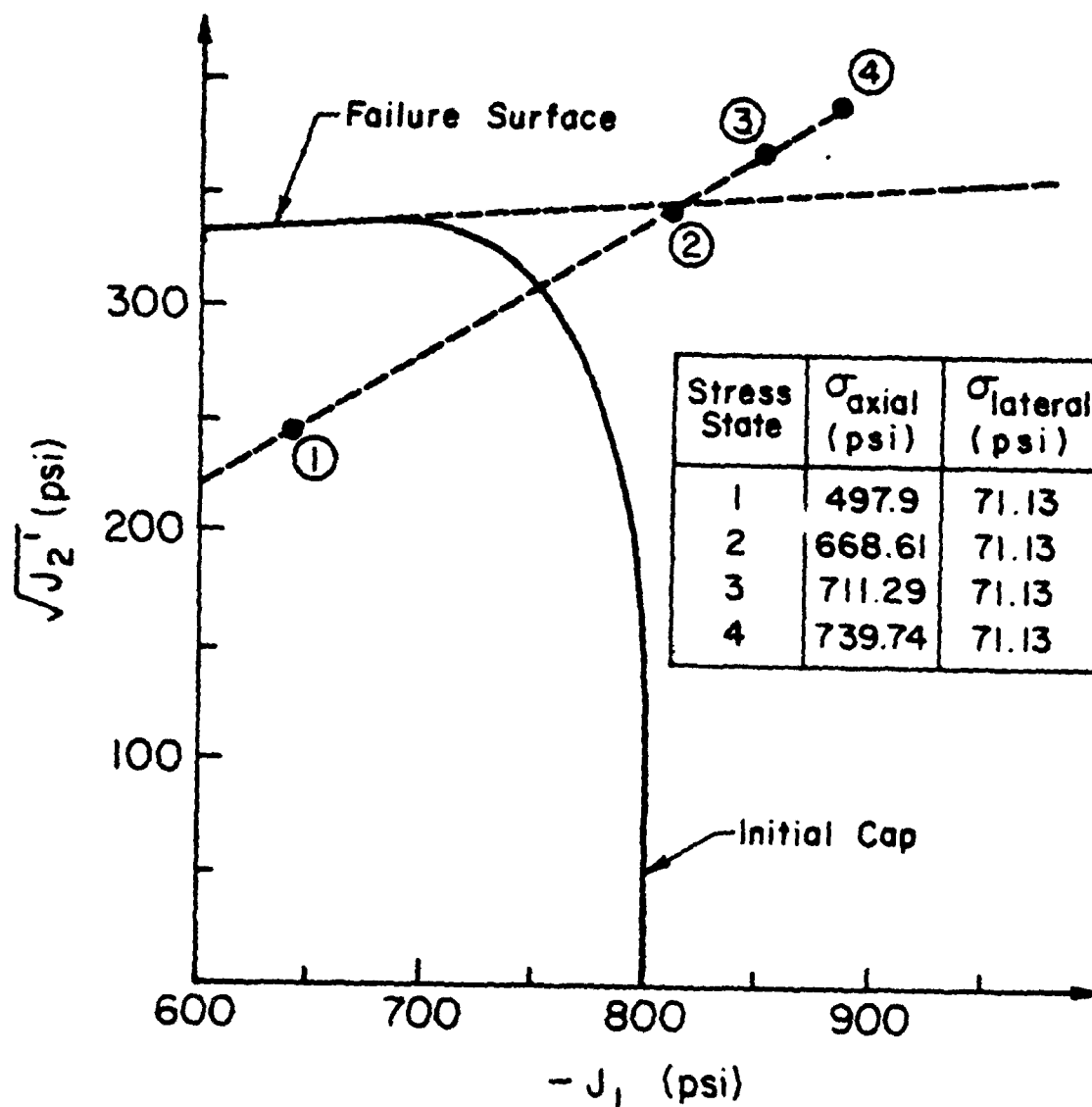
Figure 11. Axial strain response and viscoplastic cap model representation for limestone.

In accordance with previously presented guidelines, the hardening parameter D was set at $1/2|X_0|^{-1}$. The hardening parameter W as well as the fluidity parameter γ were adjusted by numerical experimentation to best match the data. No attempt was made to vary the exponent of the viscous flow function and was set at $N = 1$.

Although it is not claimed the model parameters chosen here are representative of the limestone material in any loading environment, we do assert that the representation in the range considered is fairly good. It must be said, however, that Robertson's data extended beyond the range presented here, and it was observed that, as the axial load increased, axial strains were increasing at an ever increasing rate. Such behavior may be attributed to strain softening which is not within the capabilities of the current viscoplastic model. This is illustrated in another manner in the next experiment.

Sedimentary Rock in Triaxial Stress. The viscoplastic yielding of soft sedimentary rock samples was investigated by Akai, et al. (4). Their experiments consisted of standard triaxial tests on cylindrical samples of a porous tuft described as an ideal soft sedimentary rock.

The data considered here is for four separate creep tests all with the same confining pressure and different axial loads. Each axial load is rapidly applied and held constant for the duration of the creep test, up to 8,000 minutes. Figure 12 defines the imposed stress states for each of the four tests along with the initial cap model setting and the model parameters used for this study. The measured strain history data (deviatoric strain, $\hat{\epsilon}_{11}$) reported by Akai is shown by data points in Figure 13 along with the viscoplastic model representations shown with solid lines. Here it is observed that reasonable correlation with the data was achieved in the



Elastic Moduli: $K = 125,000$ psi , $G = 60,000$ psi
 Failure Surface: $f_F = \sqrt{J_2} - (275.0 - 0.863 J_1)$, psi
 Cap Surface: $R = 0.35$, $X_0 = -800$ psi
 Cap Hardening: $D = 0.00078$ (psi)⁻¹, $W = 0.25$
 Viscous Flow: $\gamma = 0.5 \times 10^{-5}$ (min)⁻¹, $N = 1.6$,
 $f_0 = 275$ psi

Figure 12. Stress states, initial cap setting and parameters for soft sedimentary rock.

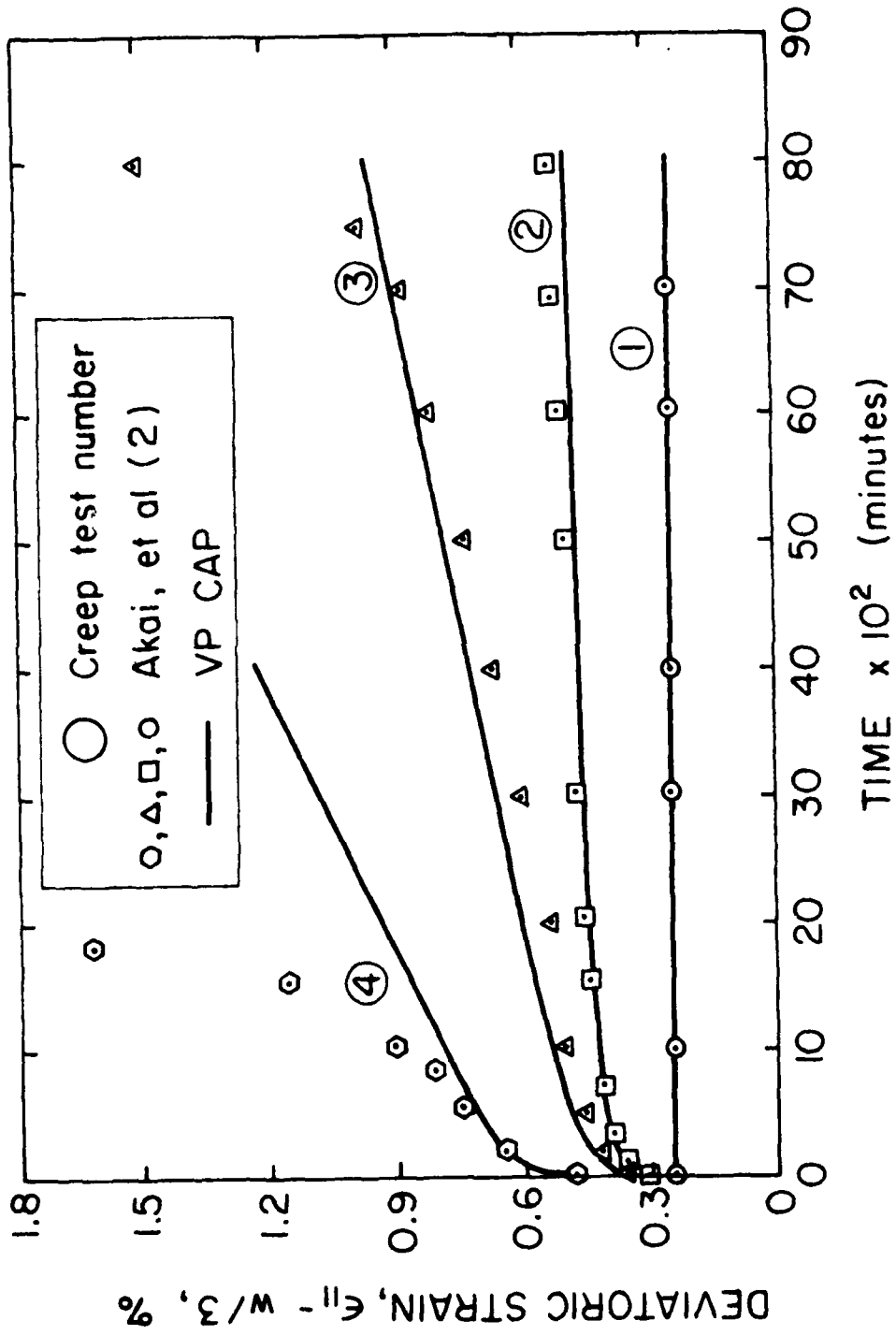


Figure 13. Deviatoric strain history responses for soft sedimentary rock.

primary and secondary creep range, but not in the tertiary creep range. This will be elaborated further after a brief discussion on the parameter identification procedure.

The elastic properties were determined by assuming no viscoplastic flow occurred while each axial load was imposed so that the initial strains were elastic. As shown in Figure 12, the initial cap setting was taken well into the compression range with $\chi_0 = -800$ psi and $R = 0.35$ along with a standard linear Drucker-Prager failure surface. The motivation for these choices were due to the observation that the strain response data exhibited continued elastic behavior for test 1, creep and then steady-state behavior for test 2, and creep and then steady-state "failure" followed by tertiary creep for tests 3 and 4. Accordingly, the initial cap setting was located between stress states 1 and 2 to insure an elastic response for test 1. The failure surface was located slightly above stress-state 2 to achieve steady-state response for test 2 and below stress-states 3 and 4 to achieve steady-state failure. Of course there is nothing unique about the particular parametric values chosen to accomplish this initial setting. In accordance with previous guidelines, the hardening parameter D was taken as a fraction of $|\chi_0|^{-1}$ and the remaining parameters W , γ , and N , shown in Figure 12, were chosen by numerical experimentation with VPDRVR program.

Returning to the model's performance shown in Figure 13, we observe the elastic response, test 1, and the steady-state viscoplastic response, test 2, are well correlated with the experimental data. In test 3, the model correlates fairly well with primary and secondary creep data. Primary creep is the early portion of the curve with decreasing strain rates (cap movement) and secondary creep is a constant strain rate (steady-state failure). The last two data points in test 3 exhibit ter-

tiary creep, i.e., increasing strain rate, which is not represented by the viscoplastic cap model. Test 4 also exhibits tertiary creep beginning almost immediately after the primary creep phase. Again, tertiary creep is not represented by the viscoplastic cap model.

From these comparisons we conclude that the present viscoplastic cap model is capable of simulating elastic, primary creep and secondary creep behavior but not tertiary creep. The inability of the viscoplastic model to simulate tertiary creep is not a question of readjusting the parameters, but rather, it is an inherent limitation of the functional forms defining the model, i.e., the present model can only respond with constant strain rates once the steady-state failure condition is reached (e.g., recall Fig. 3a). One way of overcoming this limitation is to introduce strain softening into the hardening function such that after $\bar{\epsilon}$ has grown (hardened) to a specified level, a softening function is activated shrinking $\bar{\epsilon}$, and hence increasing the strain rate as the cap retracts. Another approach would be to redefine the fluidity parameter in a functional form dependent on $\bar{\epsilon}$. This idea was discussed at the end of Part 1 of this report.

Sand in Uniaxial Strain with Variable Load Rates. We now consider the last, and perhaps, the most significant experimental test for evaluating the performance of the viscoplastic model, as well as, identifying the model's parameters. This rather ingenious experimental test, conducted at the Army's Waterways Experimental Station (11), was undertaken to directly assess the effect of loading rate on the constitutive behavior of a dry remolded sand (20-40 Ottawa Sand). The sand was molded into a thin disk-shaped specimen at the bottom of a rigid cylindrical test chamber which provided lateral constraint (uniaxial strain). By means of rather elaborate ram and explosive loading devices, several specimens were pressure

loaded with different rise times ranging from approximately 0.2 to 20,000 milliseconds. Data for each test included the time history of the pressure loading and the corresponding strain history.

Due to the small thickness of the disk-shaped specimen (1.27 cm) inertial effects are negligible even for the most rapid loading rate. That is, in reference to the so-called "multiple-reflection theory", the sand-specimen thickness is designed to be sufficiently small to permit a stress wave to multiply propagate back and forth between the rigid-bottom boundary and the free-surface boundary during the loading rise time. According to the theory, inertial stresses are negligible, and therefore, the resulting stress-strain histories provide a direct representation of the constitutive behavior. This theory was independently verified by the WES investigators for their test specimens by a simple dynamic analysis (i.e., a one-dimensional wave propagation computer program using the actual loading histories and piece-wise linear stress-strain relations determined from static tests).

Figure 14 shows the pressure loading history (σ_{11} stress) along with the measured strain history for the "slow" loading rate which has a rise time of 15,000 milliseconds. At the other extreme, Figure 15 shows the stress and strain histories for the "rapid" loading rate which has a rise time of 0.2 milliseconds. The resulting stress-strain curves for both loading rates are shown in Figure 16. Here it is plainly evident that the sand specimen exhibits rate-dependent stress-strain behavior.

Intermediate loading rates with rise times on the order of 100 milliseconds gave results almost identical to the slow loading rate experiment. This leads to two important observations, (1) the non-linear stress-strain relationship for the slow loading rate is not time dependent and may be

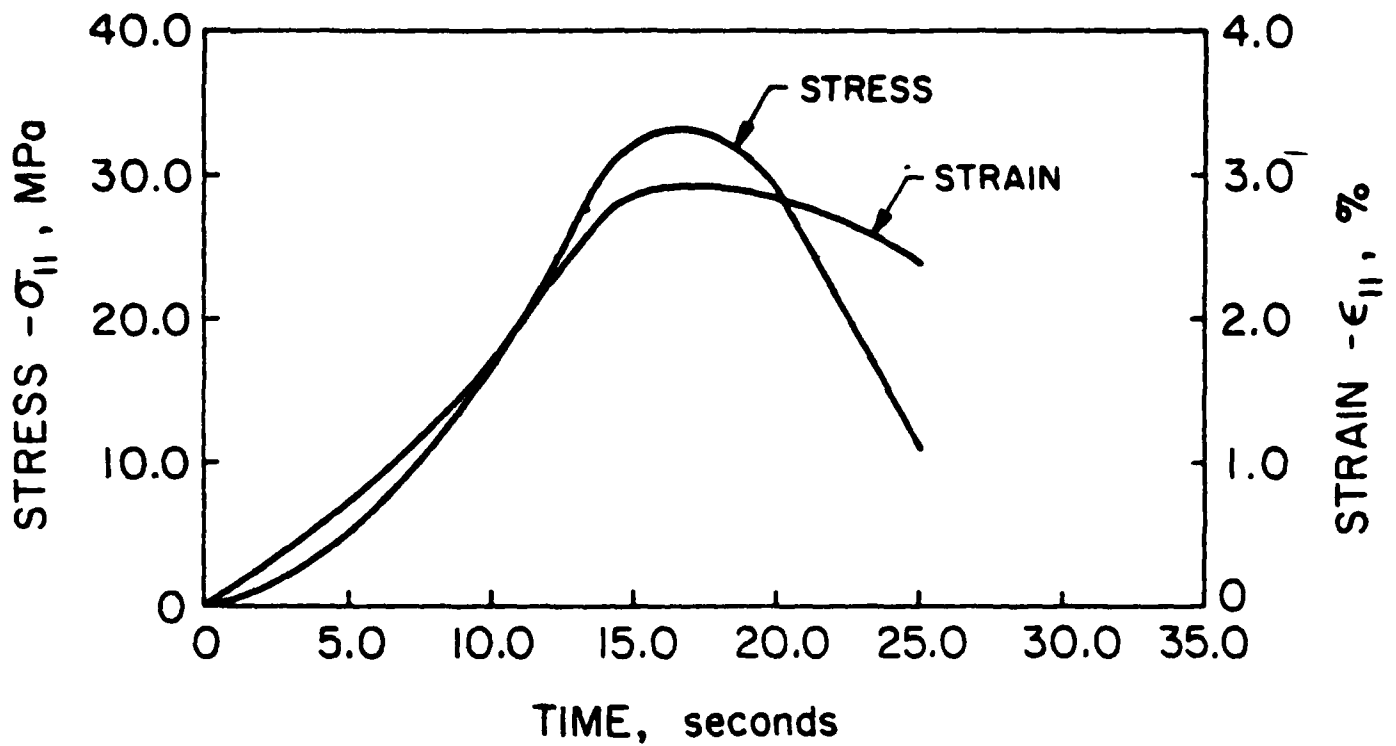


Figure 14. Slow loading stress and strain histories.

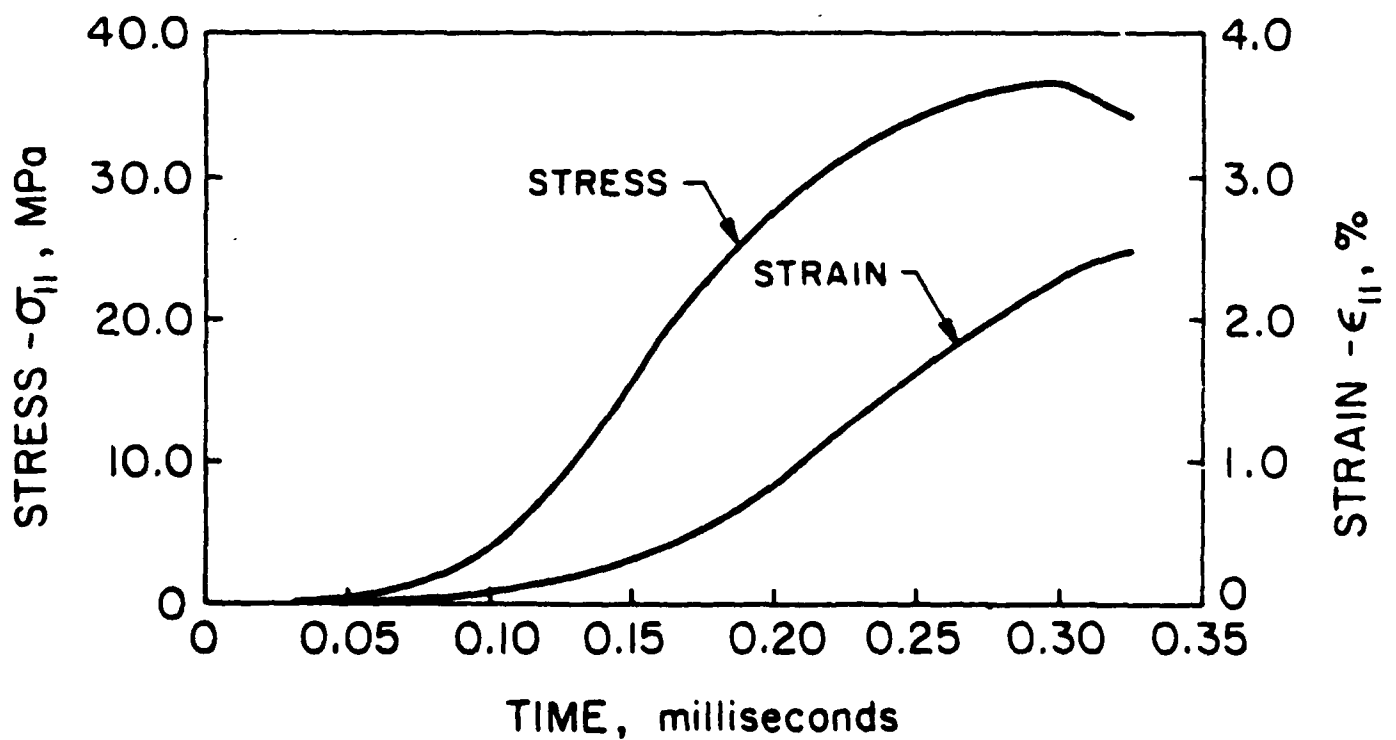
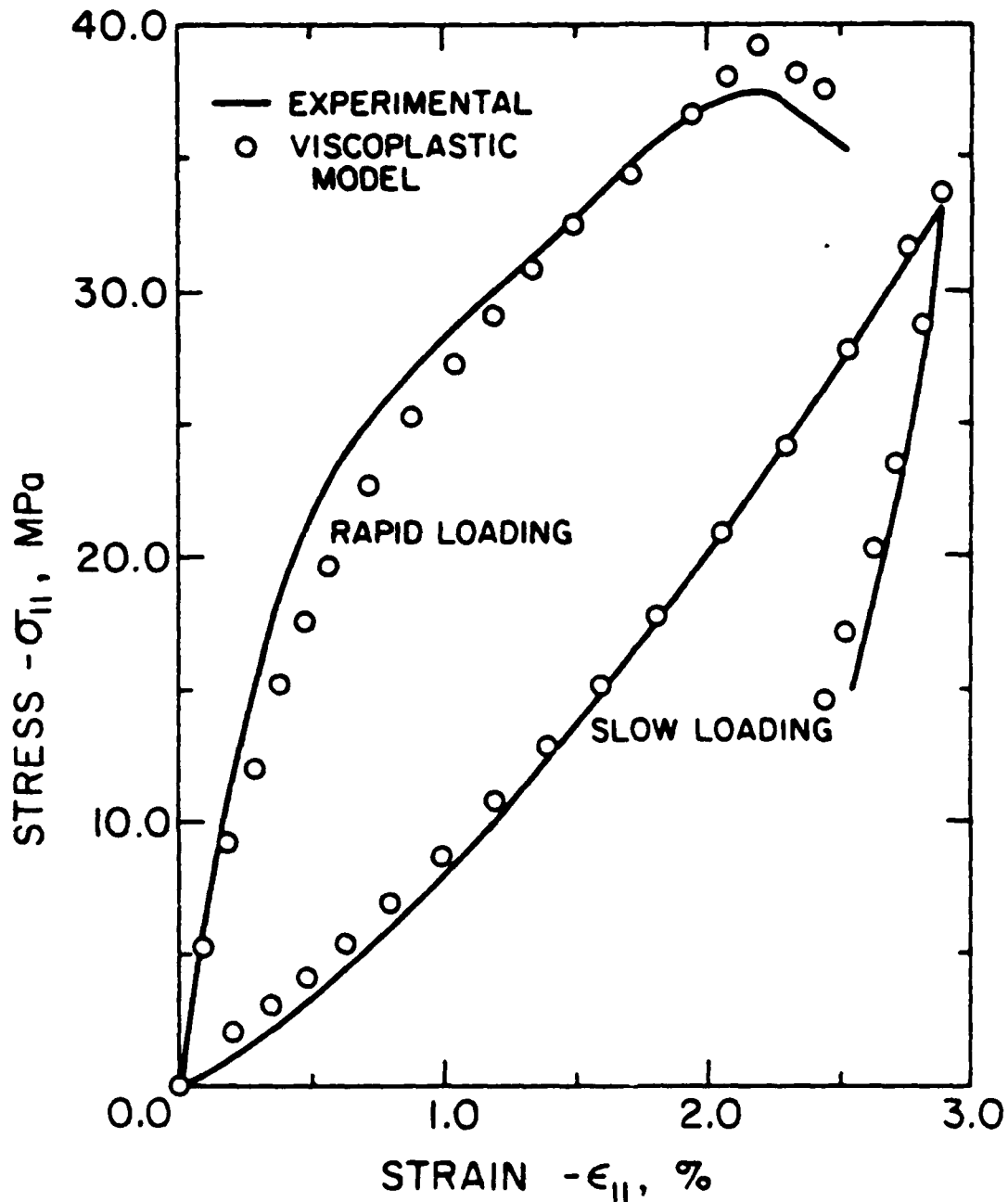


Figure 15. Rapid loading stress and strain histories.



MODEL PARAMETERS

ELASTIC: $K = 3530 \text{ MPa}$, $G = 1630 \text{ MPa}$

FAILURE SURFACE: $A = 5.0 \text{ MPa}$, $C = 4.5 \text{ MPa}$, $B = 0.004 \text{ MPa}^{-1}$

CAP SURFACE: $R = 2.0$, $X_0 = -0.3 \text{ MPa}$

CAP HARDENING: $W = 0.027$, $D = 0.014 \text{ MPa}^{-1}$

VISCOUS: $\gamma = 0.00002 \text{ MSec}^{-1}$, $N = 1.0$, $f_0 = 1.0 \text{ MPa}$

Figure 16. Stress-strain response for slow and rapid loading.

assumed inviscid, and (2) rate effects only become significant when the rise time approaches the sub-millisecond range. These observations will be used to great advantage in the subsequent parameter identification process.

The overall strategy for determining the model's parameters (listed in Figure 16) is based on the observation that the experimental stress-strain curve for the slow loading rate is an inviscid-plastic response.

Accordingly, all the elastic and plastic parameters can be determined from the slow loading-rate test. Once these parameters have been identified, the viscous parameters (η and N) can be determined from the rapid loading test. That is, for the slow-loading trial simulations, $\dot{\epsilon}$ is taken sufficiently large to ensure complete viscoplastic flow (i.e. inviscid-plastic response). In other words, there is some lower limit on $\dot{\epsilon}$ such that any value greater than this limit produces identical results. The final choice for $\dot{\epsilon}$ is directed by the rapid-loading test, i.e., $\dot{\epsilon}$ is chosen by trial and error to achieve reasonable agreement between the predicted and measured stress-strain slopes from rapid loading.

With the above understanding, the following parameter identification procedure employs the strain loading history from Figure 14 as input into the VPDRVR program. Identification begins by selecting elastic parameters to match the initial unloading slope of the slow-loading test. This slope is an elastic confined modulus graphically measured as 57,000 MPa. Using this value along with an assumed value of Poisson's ratio = 0.3, the bulk and shear modulus are set once and for all as recorded in Figure 16.

Selection of the failure surface parameters, A, B, and C (Sandler form) are guided by the observation that the unloading curve begins to exhibit a nonlinear response after a stress reduction between 5 to 10 MPa. This suggests that the elastic unloading space is rather small, hence, the

maximum failure surface height A is set at a nominally small value of 5 MPa, and the curvature parameter B is determined by trial and error to produce a re-entry point on the failure surface which approximately matches the break in the unloading curve. The parameter value for C is chosen slightly less than A in order that the difference, $A-C$, provides a very small value for the initial elastic space prior to loading. This is in conformance with the observation that no initial elastic response is observed upon initial loading. As a side comment, it was observed through numerical experimentation that a more pronounced break in the unloading curve can be achieved by reducing A and increasing B .

For the initial cap surface location, X_0 is set at an arbitrary small value to limit the size of the initial elastic space in conformance with the small $A-C$ value discussed above. The cap shape parameter R is arbitrarily set at 2.0. Numerical experimentation indicated that changes in R has little effect on the axial stress-strain curve. Its primary influence is to increase the magnitude of lateral stresses as R increases (lateral stresses were not measured in the experiments).

The most important parameters for capturing the shape of the stress-strain loading curve are the cap hardening parameters W and D . Since W represents the maximum volumetric viscoplastic strain that can be achieved, it was initially estimated as 0.03 which is approximately the maximum volumetric total strain observed in the test. As previously discussed, it is generally recommended to choose $D|X_0| = 0.5$. Decreasing D or W results in increased stress magnitude, i.e., a steeper stress-strain loading curve. After several trials, the final values selected are $W = 0.027$ and $D|X_0| = 0.047$. This completes the identification of elastic and plastic parameters.

During the above identification process, the fluidity parameter τ was set at a relatively large value to ensure inviscid responses for the slow loading-rate test ($\dot{\epsilon} = 1.0 \times 10^{-4}$ millisecond⁻¹). After the final elastic and plastic parameters were chosen, τ was repeatedly reduced to ascertain at what value of τ the slow loading begins to exhibit a small viscous response which did not differ from the inviscid response by more than 1%. This value of τ was determined to be 0.02×10^{-4} milliseconds⁻¹. Therefore, this value is a lowerbound on the final value of τ that may be selected to best fit the rapid-loading test.

The last step in the identification process is to simulate the rapid-loading test using the strain history data in Figure 15 for input into the VPDRVR program and ascertaining the viscous parameters γ and N to best match the rapid-loading stress-strain curve, all other parameters remaining the same. Here N was set to 1.0 (not varied) and the final choice for γ is 0.2×10^{-4} millisecond⁻¹, an order of magnitude greater than the lower bound established above. As a final check, the slow-loading test was rerun with the final parameters and identical results were obtained. Moreover, intermediate-loading rates with rise times on the order of 100 milliseconds were run, and the resulting stress-strain responses did not differ significantly from the slow-loading rate (i.e., in conformance with experimental observations).

Upon examining Figure 16, it is evident that the viscoplastic cap model accurately reflects the test data. For the slow-loading test, the cap surface continually moves with the stress state producing a stiffening stress-strain response as shown. Since the stress state is on the cap surface during loading, the immediate unloading response is initially elastic prior to re-entering the failure surface. On the other hand, for the fast-

loading rate, the cap surface lags behind the loading stress state producing an "apparent" softening stress-strain response (of course, this is really a time-dependent effect). Just prior to unloading, the stress state is well above the cap surface, thus when unloading occurs, the stress state remains in the viscoplastic domain producing additional strain accumulations as shown. The correlation between the model's performance and the observed performance is truly quite remarkable, particularly with regard to matching the rapid-loading behavior characteristic of ground shock problems.

Summary and Recommendations

Summary and Conclusions. In Part I of this report a theoretical formulation for viscoplastic tension cutoff was developed based on a J_1 stress criterion. For completeness, this formulation was presented with the previous CAP75 viscoplastic formulation (1) providing a complete description of viscoplastic behavior for tension cut-off, failure surface, and cap hardening. A numerical solution strategy for the complete model was presented and coded in the computer program VPDRVR (Appendix). This algorithm employs a variable Crank-Nicolson time integration scheme together with Newton-Raphson iteration procedure to solve for the six-component stress history resulting from an arbitrary six-component strain loading schedule. Also, the program solves the inverse problem, i.e., stress loading input strain history output.

The new tension-cutoff algorithm was tested against an exact solution for the case of uniaxial-stepped-strain loading. Perfect agreement was obtained. It was concluded that the fluidity parameters in the tension domain should be at least an order of magnitude larger than that in the

viscoplastic cap model is well suited for capturing the time-dependent behavior of soils and rocks over a wide range of loadings. Future enhancements of the model can easily overcome the shortcomings noted above.

Future Recommendations. Recommendations for future efforts are divided into two main areas; "model enhancement" and "automated parameter identification". With regard to model enhancement, two improvements are suggested. First and foremost it is recommended to generate the appropriate functional forms of the model to provide the capability of simulating tertiary creep. This could be done by introducing a history dependent function for the fluidity parameter and/or a strain softening function for the cap. Sufficient experimental data currently exists to meaningfully undertake this enhancement. The second enhancement is concerned with simulating tension damage accumulation associated with cyclic loading. Again, this could be done with special functional forms for the tension fluidity parameter and/or softening functions for the tension failure surface. However, to meaningfully undertake this effort, additional experimental data is required.

Lastly with regard to automated parameter identification, it is recommended to re-structure the VPDRVR program into an interactive, user-friendly, identification program. For "ideal" data the program would determine all the model parameters with very little assistance from user. For "non-ideal" data a close interaction between the user and the computer is the best approach. Here it is envisioned that the user would specify several constraints (e.g., slope of unloading curve, initial size of elastic domain, etc.) along with both stress and strain response histories. A first estimate of the parameters would be determined by the program with an over-ride option by the user. Thereafter, the user would specify one or

more parameters to be optimized, and the program would respond with the current optimum value of the varied parameter along with diagnostic data and graphs illustrating the effects of the parameter. Stepping along in this interactive fashion, i.e. changing one parameter at a time, a final solution can be obtained in a matter of a few minutes, instead of weeks by a batch oriented trial and error approach. Moreover, the intermediate diagnostic data is of tremendous educational value with regard to understanding the model's behavior.

In closing, it is worthwhile to repeat that the viscoplastic cap model has been shown to perform extraordinarily well with experimental data over a wide range of loading environments, as well as, for a variety of geological materials. No other time-dependent constitutive model has exhibited this degree of generality. Accordingly, it is highly recommended to pursue the future development of this model along the lines suggested above.

REFERENCES

1. Katona, M.G. and M.A. Mulert, "A Viscoplastic Algorithm for CAP75," Report to Naval Civil Engineering Laboratory, Contract No. N68305-80-C-0031, Port Hueneme, CA, Sept. 1981.
2. Perzyna, P., "Fundamental Problems in Viscoplasticity," *Advances in Applied Mechanics*, Vol. 9, 1966, pp. 244-368.
3. Sandler, I.S. and D. Rubin, "An Algorithm and a Modular Subroutine for the CAP Model," *Int. Journal for Numerical and Analytical Methods in Geomechanics*, Vol. 3, 1979, pp. 173-186.
4. Akai, K., T. Adachi and K. Nishi, "Mechanical Properties of Soft Rocks," IX Conference on Soil Mech. Found. Eng., Tokyo, Vol. I, 1977, pp. 7-10.
5. Zienkiewicz, O.C., et al., "Associated and Non-Associated Viscoplasticity and Plasticity in Soil Mechanics," *Geotechnique*, Vol. 25, No. 4, 1975, pp. 671-689.
6. Cormeau, I., "Numerical Stability in Quasi-Static Elasto/Visco-Plasticity," *Int. Journal for Numerical Methods in Eng.*, Vol. 9, 1975, pp. 109-127.
7. Hughes, T.R., and R.L. Taylor, "Unconditionally Stable Algorithms for Quasi-Static Elasto/Viscoplastic Finite Element Analysis," *Int. Journal Numerical Methods in Engineering*. (to be published).
8. Chen, W.F., "Plasticity in Reinforced Concrete," McGraw-Hill, New York, New York, 1982.
9. Whitman, L., "Visco-Damage Tension Model of Rocks for Ground Shock Calculations," Weidlinger Associates, Report to Defense Nuclear Agency, DNA 5271F, 1980.
10. Robertson, E.C., "Creep of Solenhofen Limestone Under Moderate Hydrostatic Pressure," Rock Deformation, *Mem. Geol. Soc. Amer.*, Vol. 79, 1960, pp. 227-244.
11. Jackson, J.G., et al., "Loading Rate Effects on Compressibility of Sand," U.S. Army Waterways Experiment Station, Report No. SL-79-24, November, 1979.

APPENDIX A

PROGRAM VPDRVR: INPUT INSTRUCTIONS

This Appendix provides input instructions for the VPDRVR program which exercises the viscoplastic cap model with tension cutoff. Only a very minor change to the original input instructions (1) are needed to define the tension cutoff parameters. These changes are on one card (Group D, Card 10) which is extended to define the tension fluidity parameters γ_T and γ_G and the hydrostatic tension cutoff value T .

For convenience, the entire set of input instructions along with tension cutoff input is given here. The program documentation and benchmark problems given in Reference (1) remain valid and are not repeated here. Benchmarks for tension cutoff are given in Part I of this report.

Input data cards are grouped in the following categories:

- A. (Cards 1 and 2): Heading and Master Control
- B. (Cards 3, 4, and 5): Elastic functions/parameters
- C. (Cards 6, 7, 8, and 9): Plastic function/parameters
- D. (Card 10): Viscous functions/parameters and tension cutoff
- E. (Cards 11, 12): Loading schedules for stress or strain.

USER INPUT INSTRUCTIONS

A. Problem Initiation, Heading and Master Control Cards.

Card 1. (15A4) Heading

<u>Columns</u>	<u>Variable</u>	<u>Entry Description</u>	<u>Notes</u>
01-60 (15A4)	TITLE	Descriptive problem title, (program terminates if TITLE(1) = STOP).	(1)

Card 2. (4I5, A1, 2F10.0) Master Controls

<u>Columns</u>	<u>Variable</u>	<u>Entry Description</u>	<u>Notes</u>
01-05 (15)	LTYPE	Loading type identification; = 0, strain loading. = 1, stress loading.	(2)
06-10 (15)	NTSEG	Number of time segments to define loading, (Default = 1, Maximum = 30).	(3)
11-15 (15)	ITMAX	Number of Newton-Raphson iterations, (Default = 10).	(4)
16-20 (15)	KPRINT	Output print control; = 0, standard response output = 1, above plus iteration parameters = 2, above plus yield function values. = 3, above plus iterative correction vector = 4, above plus Jacobian matrix.	(5)
20-21 (A1)	IPLOT	Plot control for response data written to unit 11: = Y (YES) Data written to unit 11 = N (NO) Not written	(6)
22-31 (F10.0)	THETA	Crank Nicolson integration parameter; $0 \leq \theta \leq 1.0$	(7)
32-41 (F10.0)	CONVRG	Convergence tolerance for Newton-Raphson iteration, (Default = 0.01, i.e. 1% relative error).	(8)

B. Elastic Function and Parameter Cards

Card 3. (2I5) Selection of Elastic Functions

<u>Columns</u>	<u>Variable</u>	<u>Entry Description</u>	<u>Notes</u>
01-05 (15)	IFBMOD	Selection of bulk modulus function, $K(J_1)$: = 1, $K(J_1) = BDATA(1)$, (linear) = 2, $K(J_1) = BDATA(1)/(1-BDATA(2))*$ $(1-BDATA(2)*EXP(BDATA(3)*J_1))$ (Default = 1)	(9)
06-10 (15)	IFSMOD	Selection of shear modulus function, $G(J_2)$: = 1, $G(J_2) = SDATA(1)$, (linear) = 2, $G(J_2) = SDATA(1)/(1-SDATA(2))*$ $(1-SDATA(2)*EXP(-SDATA(3)*J_2))$. (Default = 1)	(10)

Card 4. (7F10.0) Bulk modulus parameters, BDATA

<u>Columns</u>	<u>Variable</u>	<u>Entry Description</u>	<u>Notes</u>
01-10 (F10.0)	BDATA(1)	First bulk modulus parameter.	(11)
11-20 (F10.0)	BDATA(2)	Second bulk modulus parameter.	
21-30 (F10.0)	BDATA(3)	Third bulk modulus parameter.	

Card 5. (7F10.0) Shear modulus parameters, SDATA

<u>Columns</u>	<u>Variable</u>	<u>Entry Description</u>	<u>Notes</u>
01-10 (F10.0)	SDATA(1)	First shear modulus parameter	(12)
11-20 (F10.0)	SDATA(2)	Second shear modulus parameter	
21-30 (F10.0)	SDATA(3)	Third shear modulus parameter	

p

C. Plastic Function and Parameter Cards

Card 6. (4I5, G10.0) Selection of CAP75 functions

<u>Columns</u>	<u>Variable</u>	<u>Entry Description</u>	<u>Notes</u>
01-05 (I5)	IFFAIL	Selection of failure surface function $f_F = \sqrt{J_2 + 9F_1 (J_1)}$: = 1, $9F_1 = -FDTATA(1) + FDATA(2)*J_1$. = 2, $9F_1 = -FDATA(1) + FDATA(2)*$ $EXP(FDATA(3)*J_1)$. (Default = 1)	(13)
06-10 (I5)	IFCAPR	Selection of cap surface ellipse ratio R: = 0, No cap, just failure surface. = 1, $R = CDATA(1)$. = 2, $R = CDATA(1)/(1 + CDATA(2))*$ $(1.0 + CDATA(2)*EXP(CDATA(3)*EL))$.	(14)
11-15 (I5)	IFHARD	Control of cap hardening: = 0, No hardening, stationary cap. = 1, CAP75 hardening function is used: $\bar{\epsilon} = W*(EXP(D*X) - 1)$. $W = HDATA(1)$ $D = HDATA(2)$	(15)
16-20 (I5)	KAPTYP	Selection for soil or rock hardening laws: = 0, soil material. = 1, rock material.	(16)
21-30 (G10.0)	XINITL	Initial location of cap X on J_1 axis.	(17)

Card 7. (F10.0) Failure Surface Parameters, FDATA.

<u>Columns</u>	<u>Variable</u>	<u>Entry Description</u>	<u>Notes</u>
01-10 (F10.0)	FDATA(1)	First failure surface parameter.	(18)
11-20 (F10.0)	FDATA(2)	Second failure surface parameter.	
21-30 (F10.0)	FDATA(3)	Third failure surface parameter.	

* Card 8. (7F10.0) Cap Surface Parameters for R, CDATA

<u>Columns</u>	<u>Variable</u>	<u>Entry Description</u>	<u>Notes</u>
01-10 (F10.0)	CDATA(1)	First cap R parameter.	(19)
11-20 (F10.0)	CDATA(2)	Second cap R parameter.	
21-30 (F10.0)	CDATA(3)	Third cap R parameter.	

* Card 9. (7F10.0) Hardening cap parameters, HDATA.

<u>Columns</u>	<u>Variable</u>	<u>Entry Description</u>	<u>Notes</u>
01-10 (F10.0)	HDATA(1)	First hardening parameter, W.	(20)
11-20 (F10.0)	HDATA(2)	Second hardening parameter, D.	

*Skip Cards 8 and 9 if IFCAPR = 0.

D. Viscous Function and Tension-Cutoff Parameters

Card 10. (15, 6F10.0) Selection of viscous function/parameters

<u>Columns</u>	<u>Variable</u>	<u>Entry Description</u>	<u>Notes</u>
01-05 (15)	IFVISC	Selection of viscous function : = 1, $\phi = (f/ANORM)**EXPN$. = 2, $\phi = EXP((f/ANORM)**EXPN) - 1$. (Default = 1)	(21)
06-15 (F10.0)	EXPN	Exponent in ϕ function, (Default = 1.0).	(22)
16-25 (F10.0)	GAMMA	Fluidity parameter, γ .	(23)
26-35 (F10.0)	ANORM	Normalizing constant in ϕ function, (Default = max(FDATA(1), 0.01)	(24)

- Card 10 continued on next page -

D. Card 10 continued (tension cutoff parameters)

<u>Columns</u>	<u>Variable</u>	<u>Entry Description</u>	<u>Notes</u>
36-45 (F10.0)	GAMMAB	Fluidity parameter for volumetric tension cutoff, γ_T Default = γ	(a)
46-55 (F10.0)	GAMMAG	Fluidity parameter for deviatoric tension cutoff, γ_G Default = $10.0 * \gamma_T$	(b)
56-65 (F10.0)	TCUT	Hydrostatic tension cutoff limit, T	(c)

Notes a, b, and c for Card 10.

- (a) To simulate rapid volumetric stress release, GAMMAB (γ_T) should be taken significantly greater than GAMMA (γ) which controls the viscoplastic flow in the cap/failure regions.
- (b) In order to have deviatoric stresses release at the same rate as volumetric stresses, set $\gamma_G = 9K_0 \gamma_T / G_0$, where K_0 and G_0 are bulk and shear elastic moduli. Typically γ_G should be an order of magnitude greater than γ_T .
- (c) The tension cutoff value TCUT (or T) triggers tension cutoff whenever $J_1 - T > 0$. Accordingly, a sensible choice for T is in the range $0 < T < FCUT$. FCUT is where the failure surface intersects the J_1 axis. If it is desired to deactivate the tension cutoff procedure entirely, set $T \gg FCUT$. To insure that TCUT is not specified within the cap domain, the program checks that $TCUT \geq L_0$. If this is not satisfied, the program resets $TCUT = L_0$ and is noted on the printed output.

E. Input Loading Schedule and Time Steps.

Repeat card set 11 and 12 NTSEG times; NS = 1, NTSEG

Card 11 (F10.0, 215) Time segment, number of steps, print control.

<u>Columns</u>	<u>Variable</u>	<u>Entry Description</u>	<u>Notes</u>
01-10 (F10.0)	TS(NS)	Time at end of segment NS.	(25)
11-15 (15)	NUMDT(NS)	Number of times steps within time segment NS. (Default = 10)	(26)
16-20 (15)	IPRNT(NS)	Print interval for standard output: = 1, every time step prints output. = n, every nth step prints. (Default = 1)	(27)

Card 12. (6F10.0) Stress or strain load vector at time TS(NS).

<u>Columns</u>	<u>Variable</u>	<u>Entry Description</u>	<u>Notes</u>
01-10 (F10.0)	PLOAD(1,NS)	σ_{11} (or ϵ_{11}) at TS(NS).	(28)
11-20 (F10.0)	PLOAD(2,NS)	σ_{22} (or ϵ_{22}) at TS(NS).	
21-30 (F10.0)	PLOAD(3,NS)	σ_{33} (or ϵ_{33}) at TS(NS).	
31-40 (F10.0)	PLOAD(4,NS)	σ_{12} (or ϵ_{12}) at TS(NS).	
41-50 (F10.0)	PLOAD(5,NS)	σ_{13} (or ϵ_{13}) at TS(NS).	
51-60 (F10.0)	PLOAD(6,NS)	σ_{23} (or ϵ_{23}) at TS(NS).	

END OF INPUT FOR ONE PROBLEM

Commentary Notes with Input Instructions:

1. Problems may be run back-to-back. Terminate the last problem by writing STOP in columns 1 to 4.
2. Strain loading implies the six components of strain will be specified individually during the loading schedule. Similarly, stress loading implies the six components of stress will be individually specified.
3. For either stress or strain loading, NTSEG is the desired number of time segments to define the loading histories in a piecewise linear fashion.
4. Generally 10 iterations is more than sufficient to achieve convergence. If convergence is not achieved, it is a strong indication that the time step is too large. Note that convergence of the Newton-Raphson procedure does not guarantee accuracy. Accuracy can only be assured by repeatable solutions with smaller time steps.
5. Standard output includes stress or strain responses, cap location, number iterations to converge, stress invariants, and type of response. For KPRINT > 0, additional information is given primarily for debugging purposes.
6. Standard response data is written to unit 11 for subsequent plotting on a CALCOMP plotter. Subroutine GRAPH is used for plotting and may be removed or replaced if desired.
7. For THETA = 0., the solution algorithm is explicit resulting in linear equations (i.e. no Newton-Raphson iteration). For THETA > 0, the algorithm is implicit and generally more accurate for a given time step size, but requires Newton-Raphson iteration. For THETA \geq 0.5, the algorithm is unconditionally stable.
8. The convergence tolerance, CONVRG, is tested against the ratio formed by the norm of the correction vector for stress (or strain) divided by the norm of the stress (or strain) vector. Norms are Euclidean.
9. The nonlinear bulk modulus function given by IFBMOD = 2 is taken from CAPDRIVER (NCEL Program). It is a function of J_1 (first stress invariant) and is treated the same for loading or unloading. Additional functions may be added to program in FUNCTION DI(I,J).
10. The nonlinear shear modulus function given by IFSMOD = 2 is a function of J_2 , second deviator stress invariant (see Note 9).
11. For future program expansion, BDATA is dimensioned to 7 to allow incorporation of higher order nonlinear functions.
12. SDATA is dimensioned to 7 (see above).
13. For IFFAIL = 1, the failure surface is standard Drucker-Prager (or Von Mises if FDATA(2) = 0.0). For IFFAIL = 2, the failure surface is the

exponential form suggested by Sandler for CAP75. Additional functional forms may be added to the program in FUNCTION FG1.

14. By setting IFCAPR = 0, the plasticity model is governed by only the failure surface. For IFCAPR = 1 or 2 the cap surface is included with R given by the corresponding functional form. Additional functional forms for R may be added to program in FUNCTION FRCAP. (Note for IFCAPR = 2, $R = R(EL)$ where EL is "L" of cap).
15. If desired, a nonhardening cap surface may be used by setting IFHARD = 0. Otherwise the CAP75 hardening function is employed. New hardening functions can be employed by modifying SUBROUTINE CAP75.
16. See Part 1 for the special hardening rules for soils (KAPTYP = 0).
17. The initial location of X defines the starting position of the cap surface. The program checks that XINITL is not greater than FCUT, i.e. the intersection of the failure surface with J1 axis. If it is, XINITL is automatically reset slightly less than FCUT. Note, the so-called Von Mises Transition employed by Sandler is not included in this development. Thus, if it is desired to obtain steady-state viscoplastic solutions to exactly match CAP75 plasticity solutions, XINITL should be chosen so that the initial L location is not greater than zero.
18. The "standard Sandler" CAP75 failure surface is the form given by IFFAIL = 2. In which case FDATA(1) = A, FDATA(2) = C, and FDATA(3) = B.
19. The "standard Sandler" CAP75 cap surface parameter is the form given by IFCAPR = 1, i.e., CDATA(1) = R.
20. If IFHARD = 0, HDATA(1) and HDATA(2) are read but not used. If IFCAPR = 0, cards 8 and 9 are not read. HDATA as well as FDATA and CDATA are dimensioned to 7 for future program expansion.
21. For geological materials IFVISC = 1 is generally the most popular form for the viscous function. Additional functional forms may be added to the program in SUBROUTINE PHIF.
22. EXPN need not be a whole number, but must be greater than zero.
23. GAMMA has units of inverse time, the units (e.g. seconds, hours, years) correspond to the loading time units TS in Card 11.
24. Generally the default value for ANORM is appropriate providing FDATA(1) ≠ 0.0. ANORM should not be viewed as an independent material parameter since it is always associated with GAMMA in the quotient $GAMMA/ANORM**EXPN$.
25. Up to 30 time segments may be used to define a piecewise continuous collection of straight lines to define loading. For the first time segment, the program automatically assumes initial time is zero, i.e. $TS(0) = 0.0$. Thus, $TS(1)$ is the time at the end of first segment, $TS(2)$ is the time at the end of the second segment, etc. Successive values of $TS(NS)$ must be greater than the previous value.

26. Any number of time steps may be assigned to each time segment. Accuracy/stability is controlled by the time step size so that it is good practice to repeat solutions by doubling the value of NUMDT(NS). Although the time step size may be specified differently in each time segment, it is good practice not to make changes in Δt between segments by a factor of more than 2.
27. The printout interval may be specified differently for each time segment.
28. Loading values at the end of each time segment are specified individually for each vector component of strain if LTYPE = 0, or each vector component of stress if LTYPE = 1. For the first time segment the initial loading and responses are automatically assumed zero i.e., $\sigma(0) = \epsilon(0) = 0$. Standard continuum mechanics sign conventions are observed for all input and output. For example if a uniaxial stress loading cycle is desired in which σ_{11} is compressed at a constant rate to a stress value -10.0, held constant, then reverse loaded at a constant rate to a tensile stress value of +1.0, and again held constant; we infer NTSEG = 4, and σ_{11} is described by:

```
PLOAD(1,1) = -10.0
PLOAD(1,2) = -10.0
PLOAD(1,3) = +1.0
PLOAD(1,4) = +1.0
```

and all other stress components (PLOAD) are zero.

ATE
LME